MODULAR MULTI-WIRE DRIFT CHAMBERS FOR THE TRIUMF QQD-SPECTROMETER

by

BRIGITTA MONICA FORSTER

B.Sc., University of British Columbia, 1982

A THESIS SUBMITTED IN PARTIAL FULFILLMENT OF THE REQUIREMENTS FOR THE DEGREE OF MASTER OF SCIENCE

in

THE FACULTY OF GRADUATE STUDIES

Department of Physics

We accept this thesis as conforming

to the required standard

THE UNIVERSITY OF BRITISH COLUMBIA

December 1986

In presenting this thesis in partial fulfilment of the requirements for an advanced degree at the University of British Columbia, I agree that the Library shall make it freely available for reference and study. I further agree that permission for extensive copying of this thesis for scholarly purposes may be granted by the head of my department or by his or her representatives. It is understood that copying or publication of this thesis for financial gain shall not be allowed without my written permission.

Department of Physics

The University of British Columbia
1956 Main Mall
Vancouver, Canada
V6T 1Y3

Date Dec. 19, 1986

ABSTRACT

A modular, multiwire drift chamber was built and tested in the M13 area. The resolution obtained with six sense wires, was in the horizontal drift direction σ(mean) < (79.9±.2)μm, with an angular resolution of (9.37±.02)mrads.

With the drift chamber mounted in the first wire chamber position of the QQD-spectrometer, this corresponds to a resolution of 1.97mm FWHM at the position of the scattering target.
In the vertical direction, using a charge division method, the best achieved resolution was < 2mm FWHM per wire, which gives an angular resolution of 71mrads or 15mm FWHM at the target position.
The chamber was run at rates in excess of 10^6 particles/sec.

A multi-chamber system was tested, consisting of two modular four cell drift chambers for the horizontal direction, and one eight cell modular drift chamber, located in between and rotated by 90^0, was used for the vertical position determination. The resolution for one four cell chamber was σ(mean) < (108.5±.9)μm, and for the eight cell chamber σ(mean) < (79.9±.2)μm. The angular resolution for this system was 1.37 mrad horizontally and 9.37mrads vertically; in connection with the QQD-spectrometer, this corresponds to FWHM of 0.267mm and 1.12mm respectively at the target spot.

TABLE OF CONTENTS

TABLE OF CONTENTS (continued)

TABLE OF CONTENTS (continued)

LIST OF TABLES

LIST OF FIGURES

LIST OF FIGURES (continued)

ACKNOWLEDGEMENTS

I would like to express my thanks to my supervisors Dr. R.R. Johnson and Dr. K. Erdman as well as Dr. D. Gill for encouragement and guidance during this project.

Many thanks go to John Stewart and Eddie Knight for their expert advice and continual technical assistance. I am further indebted to Dr. D. Hutcheon for inciting discussions and suggestions for the data analysis. Thanks are also due to the members of the PISCAT group.

Finally my deep appreciation goes to my husband Rolf, for his support and assistance in typing this manuscript.

CHAPTER I - INTRODUCTION

I.A. MOTIVATION FOR THIS PROJECT

At the front end of the low energy pion QQD -spectrometer at TRIUMF are presently provisions for three standard type Multi-Wire Proportional Chambers (MWPC). The spectrometer is usually running with one MWPC at the front of the first quadrupole magnet in the WC1 position (Fig. I.1), and an other MWPC at the WC3 position between the second quadrupole and the dipole magnet. The horizontal (x) and the vertical (y) readout from each chamber is used to project the position of an incoming pion back to the target.

The resolution of the spectrometer is limited partly by the intrinsic resolution of these two detectors, as well as the multiple scattering induced mainly by their window foils, and to a lesser degree the gas-contents of the chambers and the spectrometer itself. The intrinsic resolution of the MWPC's depends on their wire-spacings which are 1mm in the horizontal and 2mm in the vertical direction and the characteristics of the delay-lines which are used for the identification of the individual wires.

A second limitation is imposed by the incoming particle flux which can be tolerated by MWPC's. As a consequence, the QQD spectrometer does not operate efficiently at small forward angles.

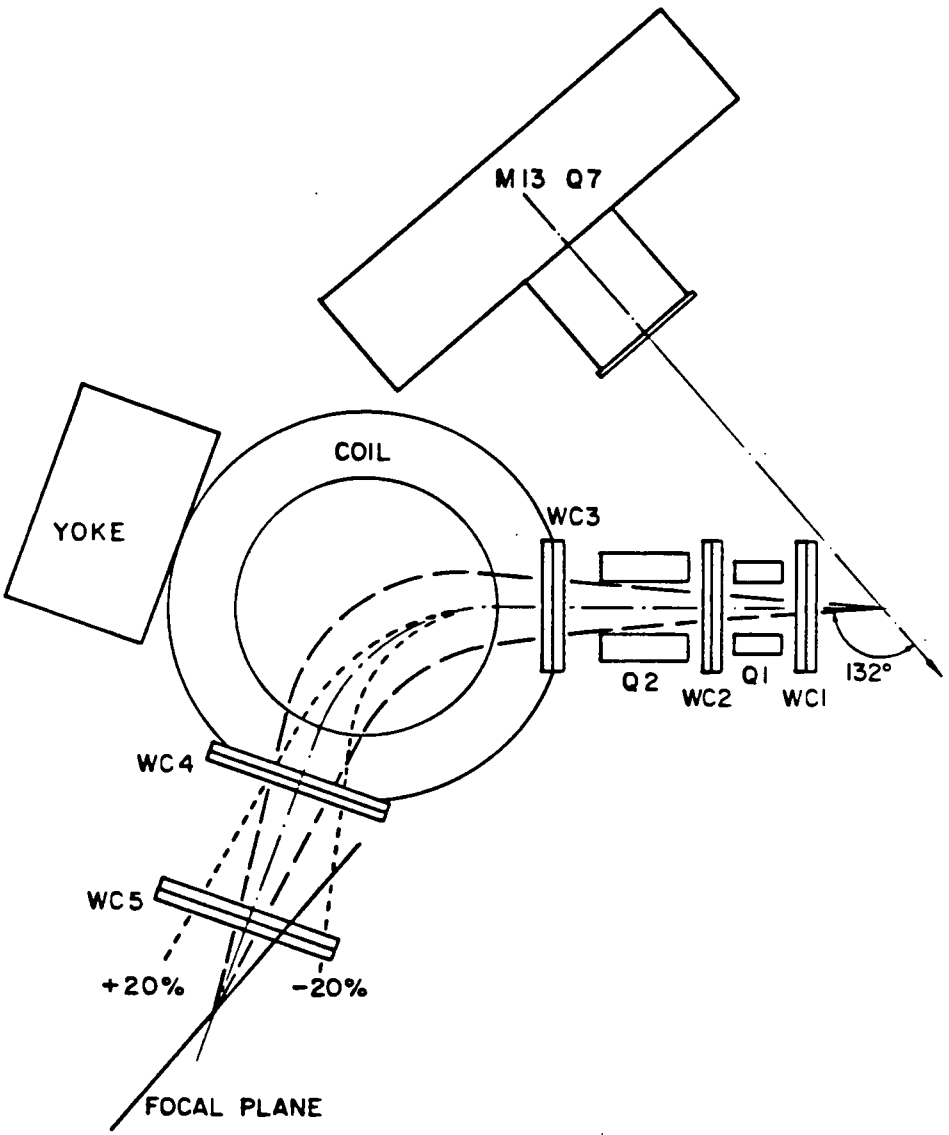

Fig. I.1

QQD spectrometer at M13 focus. All available positions for wire chambers are shown.

Single wire readout chambers could certainly overcome the rate problem, but could not simultaneously improve the resolution.

Dr. K. Erdman suggested the replacement of the two MWPCs with a drift chamber, which would offer improvements in both resolution and rates. It is the intention of this work to document the building and testing of driftchambers based on his design and to comment on possible implementations.

CHAPTER II - GENERAL PRINCIPLES OF A DRIFT CHAMBER

Drift chambers are used extensively in high energy physics. They are best known for very high spatial resolutions as well as high rate capabilities. A drift chamber consists of one or several drift cells. An individual drift cell measures a single spatial coordinate of a charged particle which traverses a suitable medium. This is achieved by exploiting the physical message provided by the electromagnetic interaction of the particle with the medium.

This chapter gives a brief review of the general principles which make drift chambers possible. It is based mainly on three review articles [1-3].

II.A. THE SINGLE DRIFT CELL

The most basic cell consists of an anode wire and a cathode plane which are kept at high voltage in the gas filled drift space. The electrons produced through ionization by a charged particle traversing the drift space drift towards the anode wire and produce an electrical signal. The drift time, that is the time difference between the anode signal and a reference time signal (given for example by plastic scintillation counters outside the drift cell) is then proportional to the drift distance Δx. A schematic picture of a single drift cell is given in Fig. II.1.

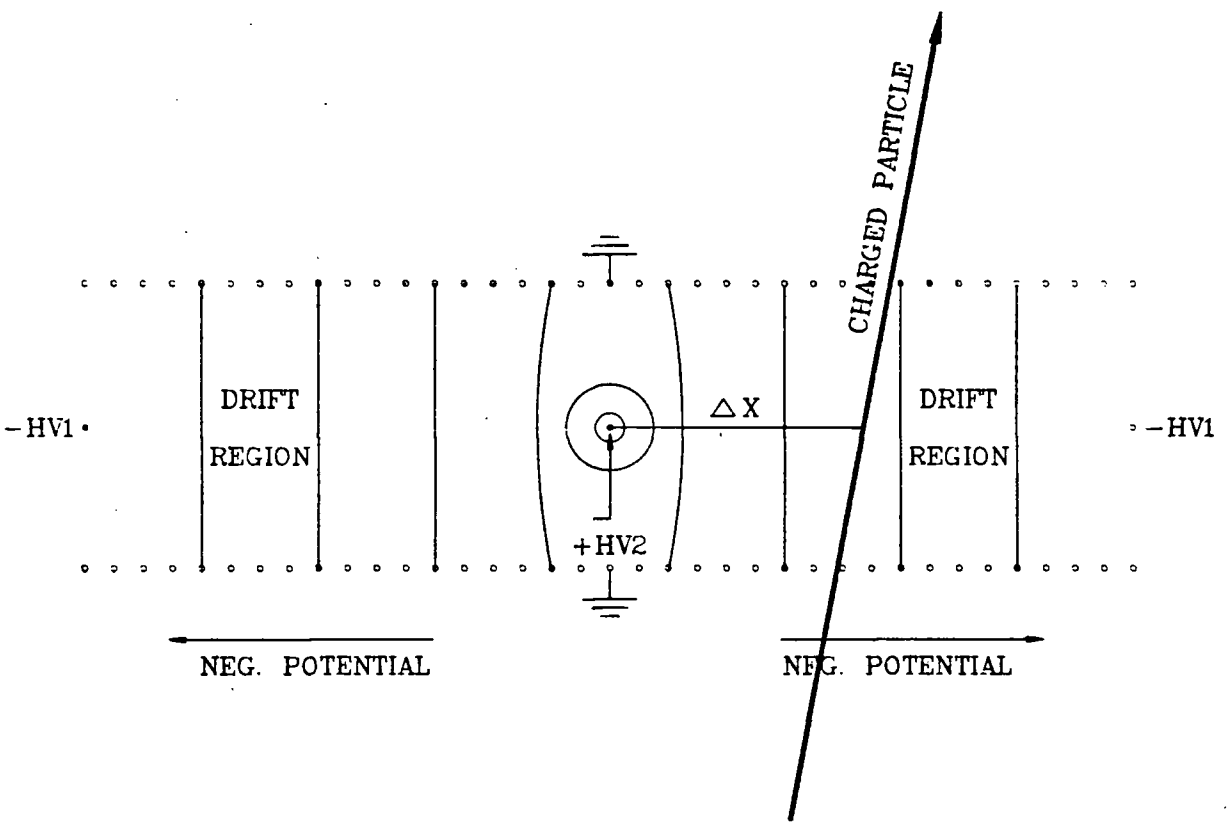

Fig. II.1

A single drift cell

For the reconstruction of the actual trajectory of a charged particle, two or more drift cells can be stacked behind each other. Alternatively, a multi-anode drift chamber can be used.

II.B. BASIC PHASES

A charged particle traversing the gas in a drift chamber ionizes along its track. The primary electrons created in this process lose their energy by further ionization and excitation of gas atoms and/or molecules until they become sensitive to the applied electric field and start to "drift". This means the electrons are accelerated by the electric field towards the anode, having multiple collisions with gas atoms and/or molecules along the way. A global motion in the direction of the electric field is superimposed on the random thermal motion. The average displacement of the electron swarm per unit time is called the drift velocity. Finally, in the immediate vicinity of an anode wire, the electric field rises rapidly. This results in an avalanche multiplication which is necessary for a measurable electric signal.

There are therefore three distinct phases which have to be taken into consideration when designing or operating a drift chamber:

II.B.1. Thermalization

The first phase encountered is the thermalization of the electrons along the path of the incident charged particle. It is this physical extension and non-uniform density of the ionized trail - due mostly to emission of delta electrons - which can limit the position accuracy of a drift cell. This phase is dominated by the original energy of the ionizing particle, and the composition as well as the pressure of the drift gas.

II.B.2. Drift Phase

After the thermalization process the electrons drift in the direction of the applied electric field. A constant value of the drift velocity makes it possible to translate the measured time difference into a spatial distance.

The value and stability of the drift velocity have direct bearing on the resolving power of the drift cell and on the maximum rate at which the cell can be operated. The drift velocity depends mainly on the homogeneity and strength of the electric field, and on the gas components and the gas pressure.

II.B.3. Avalanche Multiplication

Avalanche multiplication is induced by the rapidly rising electric field around the anode wire. This effect sets the performance limits for the time-measuring electronics, which ultimately determines the efficiency of the detector. The angular spread of the electron avalanches depends strongly on the counter gain and - to a smaller extent - on the gas mixture and anode diameter [1]. Detailed measurements have shown that this spread can be rather narrow at moderate avalanche gains and in well quenched gases. A narrow angular spread of the avalanches not only allows the detector to be run at higher rates, but also to acquire an extra space coordinate through the charge division method (See chapter III.E).

Another basic process taking place throughout the length of the drift path is the dispersion due to diffusion. It depends on the kind of gas mixture, the pressure, and the field strength and increases with the drift distance. A short basic introduction to diffusion and drift of charged particles follows in the next two sections, while more details on electric field considerations, specific gas mixtures and optimization of rates and resolution will be discussed in the respective sections of chapter III.

II.C. BASIC PROCESSES

II.C.1. Drift of Charged Particles in Gases

For ions the drift velocities w^+ increase linearly with the applied electric field up to values of several kV/cm.atm as [4]:

$$w^+ = \mu^+ E/p \qquad \text{(II.1)}$$

where p is the gas pressure and μ^+ is the ion mobility, which is specific for each ion in a given gas. The average ion energy in this region remains equal to the thermal value kT [4].

The electrons, on the other hand, can much more easily be accelerated by the applied field between collisions with gas molecules. They reach average energies far exceeding the thermal energy even at moderate fields.

Electron theory gives a simple formula for the electron drift velocity w^- [4]:

$$w^- = eE\tau/2m \qquad \text{(II.2)}$$

where τ is the mean time between collisions. Unfortunately it was found that for some gases the collision cross-section and therefore τ varies strongly with E, going through maxima and minima. This anomaly

(Ramsauer Effect) was first observed in Argon (incidentally a very popular drift gas component) and later also in Krypton and Xenon as well as several organic compounds like Methane, but not in Helium and Neon. In addition it was found [5] that even the addition of a very small fraction of another gas can modify the average electron energy and so dramatically change the drift properties.

II.C.2. Electron Diffusion

A group of electrons in a drift gas will suffer dispersion due to diffusion. A charge distribution which at time t=0 is described by a delta function, will be described at time t (along a given direction x) by a Gaussian distribution with the following standard deviation [3]:

$$\sigma_x = \sqrt{2Dt} \qquad \text{(II.3)}$$

where D is a field dependent diffusion coefficient and t is the time of drift.

It is customary to define a characteristic energy ε_k as the ratio between the diffusion coefficient and the mobility [6]:

$$\varepsilon_k = eE \frac{D}{\bar{w}} \qquad \text{(II.4)}$$

where $\bar{w}$ is the drift velocity.

In the ideal case, where the electron energy is not modified with increasing values of E, the drift velocity increases linearly with the field. Then ε_k equals its classic value kT and the space diffusion for a drift length x is given by [6]:

$$\sigma_x = \sqrt{\frac{2kTx}{eE}} \qquad \text{(II.5)}$$

This quantity is often called the thermal limit to electron diffusion.

For any gas at a given temperature T, the average electron drift velocity is given by [7]:

$$\bar{w} = -\frac{4\pi}{3} \frac{e}{mN} \frac{E}{P} \int_o^\infty \frac{v^2}{\sigma_m(v)} \frac{df_o}{dv} dv \qquad \text{(II.6)}$$

where N is the number of gas molecules per cm^3 at 1 torr, σ_m is the momentum transfer cross section, f_o is the spherically symmetric term in the expansion of the electron velocity distribution function.

If one combines II.3 and II.4 one obtains:

$$\sigma_x = \sqrt{\frac{2\varepsilon_k x}{eE}} = \sqrt{\frac{2\varepsilon_k x}{e}\frac{P}{E}}\frac{1}{\sqrt{P}} \qquad \text{(II.7)}$$

It can be seen that the diffusion in any given drift gas depends not only on E/P (since ε_k does) but also on $\frac{1}{\sqrt{P}}$.

At a given gas pressure, the diffusion coefficient is smaller for "cool" gases, i.e. gases in which the characteristic energy ε_k is small even at high E/P values. It should be noted that the given σ_x represents the width of the charge distribution, and not the error on its localization.

Furthermore, the diffusion is not always symmetric, especially at high fields. The longitudinal diffusion coefficient D_L (with respect to the drift velocity) tends to be smaller than the transverse diffusion coefficient D_T.

This classical approach does not work that well when applied to a gas mixture. Only calculations based on rigorous transport theory have accurately reproduced the experimental data.

II.C.3. Drift of Electrons in Presence of Magnetic Fields

The presence of a magnetic field other than parallel to the drift direction modifies both the drift velocity and the drift path of the electron swarm. In noble gases the drifting electrons show a broad spectrum of velocities even at moderate fields, since most of their

collisions are elastic. Consequently, in high transverse magnetic fields, the Lorentz force $\underline{v} \times \underline{B}$ will cause a wide range of deflection angles and thus impair the performance of the detector. Organic admixtures to the noble gases allow the drifting electrons to transfer energy quickly to rotations and vibrations of complex molecules. This leads to the desired narrowing of the velocity distribution for the electrons.

Drift chamber operation in strong magnetic fields will not be discussed any further here. Although all the drift chambers constructed in this thesis were tested and intended to be used in the fringe field of the TRIUMF QQD spectrometer, it has been shown that similar drift cells filled with various gas mixtures could tolerate fields as high as 0.13 Tesla before corrections to the data were necessary [8].

CHAPTER III - PRINCIPLES OF OPERATION

III.A. ELECTRIC FIELD

A homogeneous E-field is essential for a constant drift velocity throughout a drift cell. However, in the immediate vicinity of an anode, the homogeneity will cease since the E-field varies rapidly as 1/r, where r is the distance from the wire center. This leads to an avalanche multiplication which is necessary for a measurable signal. The amplification increases exponentially with applied voltage above threshold. Threshold occurs when an electron can gain enough energy between collisions to ionize a molecule in the next collision.

Since the velocity distribution is a function of the electric field and the pressure through the ratio E/P, it is extremely important to use a gas in which the drift velocity saturates at a moderate threshold. Saturation should extend to the highest values of the field, making the chamber response almost independent from local imperfections and mechanical tolerances in the placing of the cathode and the field defining wires.

In multi-wire drift chamber designs, there are often field wires at ground potential alternating with anodes (see Fig. V.1). Their function is to help to separate individual drift cells and thus to focus incoming electrons. Those field wires also prevent electrostatic coupling between anodes.

III.B. GAS MIXTURES

The composition of the gas mixture used in a driftchamber will depend very much on the specific experimental requirements; such as high rate capabilities, low working voltage, long lifetime,etc.

Noble gases are often chosen as the main component since avalanche multiplication occurs at much lower fields than with complex molecules. However, during the avalanche process excited and ionized atoms are formed. The excited noble gases can return to the ground state only through a radiative process, and the energy difference between the first excited state and the ground state, (11.6eV for Argon, 16.6eV for Neon) is well above the ionization potential of any metal used for wires or cathode planes (7.7eV for copper, 6.0eV for aluminium). This puts limits on the allowed gain for the chamber before it enters a regime of permanent discharge.

On the other hand, most organic compounds (hydrocarbons, alcohols) have many non-radiative excited states due to rotations and vibrations. Because this allows the absorption of photons in a wide energy range, the quenching efficiency of a polyatomic gas increases with the number of atoms in the molecule.

But large, complex molecules with very high quenching abilities will at the same time reduce dramatically the gas-gain at the

anode wire. The problem with very simple molecules, like carbon dioxide, is that secondary emission which may lead to a discharge, has occasionally been observed.

The polymerization of hydrocarbons, especially at high counting rates, makes it mandatory to operate the chamber in an open gas flow configuration. Non-polymerizing quenchers like methylal [$(OCH_3)_2CH_2$] are not effective against photo-ionization and secondary emission, but, if added even in small quantities will neutralize hydrocarbon-ions into a non-polymerizing species.

It is advisable to choose a gas mixture in which the drift velocity reaches an extended plateau at a specific electric field. It is then extremely important that the chamber be operated above this field threshold at all times. Characteristics of different gases and gas mixtures as well as their associated velocities, are readily available in the literature. A compilation of many works is found in Ref. [9].

The general requirements for the performance of a drift chamber depend on the detector design. A single drift cell is characterized by the applied electric field, its length to depth ratio and the potential on the anodes. As far as the drift gas is concerned, a very high drift velocity is required if the emphasis of the chamber is towards handling high rates. Better spatial resolution is achieved, if first of all the drift gas is kept at high pressure and by chosing a

slow velocity "cool" gas, where the characteristic energy ε of the electrons is close to the thermal limit $\varepsilon \sim kT$

Unfortunately, many of those very low velocity gases, like Di-methyl-ether, do not have a saturation velocity. Although very good resolution can be attained with it, the chamber has to be constantly and carefully monitored [10].

While testing the chambers built for this project it was found, that they worked well with either Argon- or Neon-hydrocarbon mixtures, as long as the noble gas content was not dropped below 50% in volume. In mixtures with more then 50% hydrocarbons, the signal to noise ratio in the electronics no longer allowed the chambers to be operated at maximum efficiencies.

Except when stated, all drift gases were mixed on site using the TRIUMF mobile mixing units. All tests were done at 1 atmosphere pressure with continuous flow. All flow meters have been individually calibrated for the pertinent gases. Methylal was only needed for the high rate tests. At these times the noble gas was bubbled through the liquid methylal which was kept at zero degrees Celsius. This corresponds to a (3 - 5)% methylal content in the noble gas.

The gas doping for the laser calibration runs is discussed in section VI.A.1.

III.C. RESOLUTION

The spatial resolution in a drift chamber is limited mainly by:

- the physical width and the statistical spread of the original ionization track
- the value and stability of the electron drift velocity
- the dispersion due to diffusion, which depends on the gas mixture as well as the gas pressure and the electric field strength.

Dispersion always increases with drift distance. Both the physical extension of the ionization track and the diffusion can be reduced by increasing the gas pressure to several atmospheres. The actual depth of the drift cell can further limit the resolution if there is a time difference between ionization clusters belonging to the same track arriving at the same wire.

III.D. HIGH RATES

The count rate is limited most severely by space charge accumulation in the drift region, and an efficiency loss caused by the finite duration of the signals, usually referred to as dead time loss.

III.D.1. Space charge

The positive ions which are generated in the gas amplification will lower the electric field strength near the anode. Due to their greater mass, ions will have a slower drift velocity than electrons. This results in a pulse height drop and could consequently affect the chambers efficiency.

Since this effect depends on the extension of the avalanche near the anode wire, the most important design parameters will be the radius of the sense wire, gas gain and gas composition.

III.D.2. Dead time

At high rates, the signals occasionally overlap and can therefore not be counted individually.

For a high rate chamber, the following design criteria should be observed:

- small wire spacing to reduce the rate per wire,
- small gap width to reduce space charge effects and reduce signal tails caused by late arriving ionization,
- low noise preamplifier to operate at low gas amplification,
- small anode radius to provide fast anode signals and to reduce local space charge,

- large bandwidth amplifier to allow fast clipping of signals,
- dead time of discriminator matched to width at base of clipped signal [11].

Finally, if the chamber is run at high rates over an extended period of time, additional care should be taken to preserve the condition of the wires in the chamber. Only highly purified gases can be used. The hydrocarbon content in the gas mixture may have to be reduced and a non-polymerizing quencher, such as Methylal, must be added.

III.E. CHARGE DIVISION

In the charge division method, the position of impacting particles is determined along the wire, through the ratio of resistances.

If Q_{up} and Q_{down} are the amounts of charge collected at the up and the down end of the sense wire respectively, the position is then given by:

$$\frac{Q_{up} - Q_{down}}{Q_{up} + Q_{down}} \cdot \frac{\text{wire length}}{2}$$

In a drift cell, the charge division method can be used to measure a second space coordinate in the y direction.
If applied to the ion signal on highly resistive cathode wires, it gives the y coordinate, but due to the low mobility of the ions the rate capability of the drift chamber would drop significantly. A more promising method would be to place resistive wires close to the anodes and process the electrostatically induced electron signal.

It has been shown by several authors [12,13,14] that drift time measurements and charge division can be performed simultaneously on the same resistive anode. Both ends of the wire are connected through capacitive decoupling directly to the input of low impedance preamplifiers. The signals are then processed separately for charge division and for timing.

The value of the anode wire resistance should be high in order to keep the noise level low and to improve the position resolution along the wire. On the other hand, a small resistance is required in order to have good linearity in the position determination and high resolution in the drift time measurement. The resolving time for the charge division method is about one electrode time constant τ for optimum position resolution and linearity [15]. (τ = RC, where R, C are the resistance and capacitance per unit length of the line). A

detailed analysis [16] has shown that the best compromise for simultaneous position and drift time resolution is achieved by [13]:

$$R = 2\pi (L/C)^{1/2}$$

where L stands for the inductance per unit length of wire. This corresponds to the critical damping condition for transmission lines. The charge measurement is seriously limited by the input impedance of the amplifier, the input stage of which should be a current amplifier [16].

CHAPTER IV. - THE MODULAR MULTIWIRE DRIFT CHAMBER (MMDC)

IV.A. THE CONCEPT

The first attempts at the new QQD front end detector were the construction and the testing of a more conventional multi-wire drift chamber. Out of the collected experiences during that project grew the design of modular drift cells. Rather than being limited to a single instrument which is fixed by its rigid dimensions and design specifications, modular type drift cells are capable of providing versatile detector combinations which can be easily built, maintained, and repaired whenever the need arises. They can also be adapted to different tasks which may require the change of the characteric depth of a drift cell, as well as the replacements of wires by new ones of different materials or/and diameters.

With the exception of the actual printing of the circuit boards, all of these drift chambers were strung, assembled, altered, and calibrated at TRIUMF, without requiring sophisticated tools or equipment.

IV.B. CONSTRUCTION OF MODULES

The modular drift chambers were constructed entirely out of 1.5 mm thick printed circuit boards. The G-10 material is cut into identical frames with a 50 mm x 50 mm opening. 12 positioning holes are drilled symmetrically throughout the border. Only two circuit designs are necessary:

The type A boards (see Fig. IV.1a) contain the field defining wire cage and are used as the two end boards for the chamber. Field wires are 100 μm Cu-Be, strung at a tension of 120 grams and are 5 mm apart from each other. The voltage drops evenly from the two cathodes on either side of the frame towards the centre wire, which is grounded. Potential differences between wires are obtained through a chain of 12 MOhm resistors which are soldered directly onto the boards. The inside edges of the circuit boards, which define the cathode planes, are painted with a conducting graphite solution.

The type B boards (see Fig. IV.1b) have the centre electrical contact pins offset towards one side. They are used for both the sense wires (anodes) and the potential wires, which are kept at ground potential. Anode wires are 20 μm thick gold plated tungsten and are strung at a tension of 50 grams. The two anodes used for the charge division measurements are 20 μm thick high resistance (3.5 kΩ/m) NiCr wires at a tension of 10 grams.

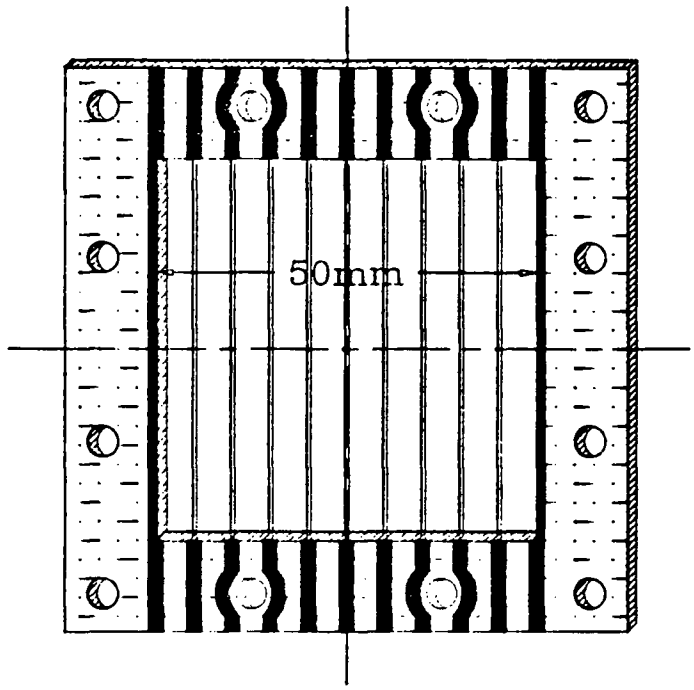

type A board

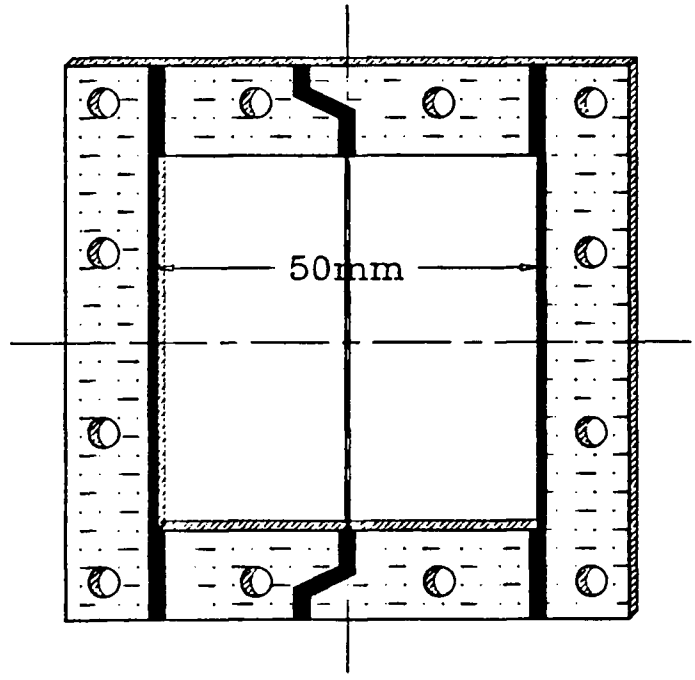

type B board

Fig. IV.1

The two basic MMDC frames

The potential wires are 100 μm thick Cu-Be at a tension of 120 grams. Care must be taken that the contact pin offset on the boards which are strung with potential wires are all towards the same side, while for all the sense wires the boards have to be rotated by 180 degrees. This gives a maximum distance between the contact pins of the grounded potential wires and the pins for the anodes (which carry high positive potential), thus reducing the chance of sparking between them. As before, the inside edges of the frames which define the cathode planes are painted with a conducting graphite solution.

For stringing the wires, a stringing jig was used (Fig.IV.2). The printed board is positioned with four locating pins onto a sled which moves laterally. The wire sits in V-grooves located at either end of the circuit board and is brought to the required tension. A three position toggle determines the wire position either at centre or 200 μm to the right or left of it. The tolerance of the jig was measured to be < 10 μm.

IV.C. ASSEMBLY

The chamber is assembled by pushing threaded nylon rods through the positioning holes all around the circuit boards. Distances between anodes and potential wires, which determine the characteristics of a single driftcell, are set by nylon washers which were machined to

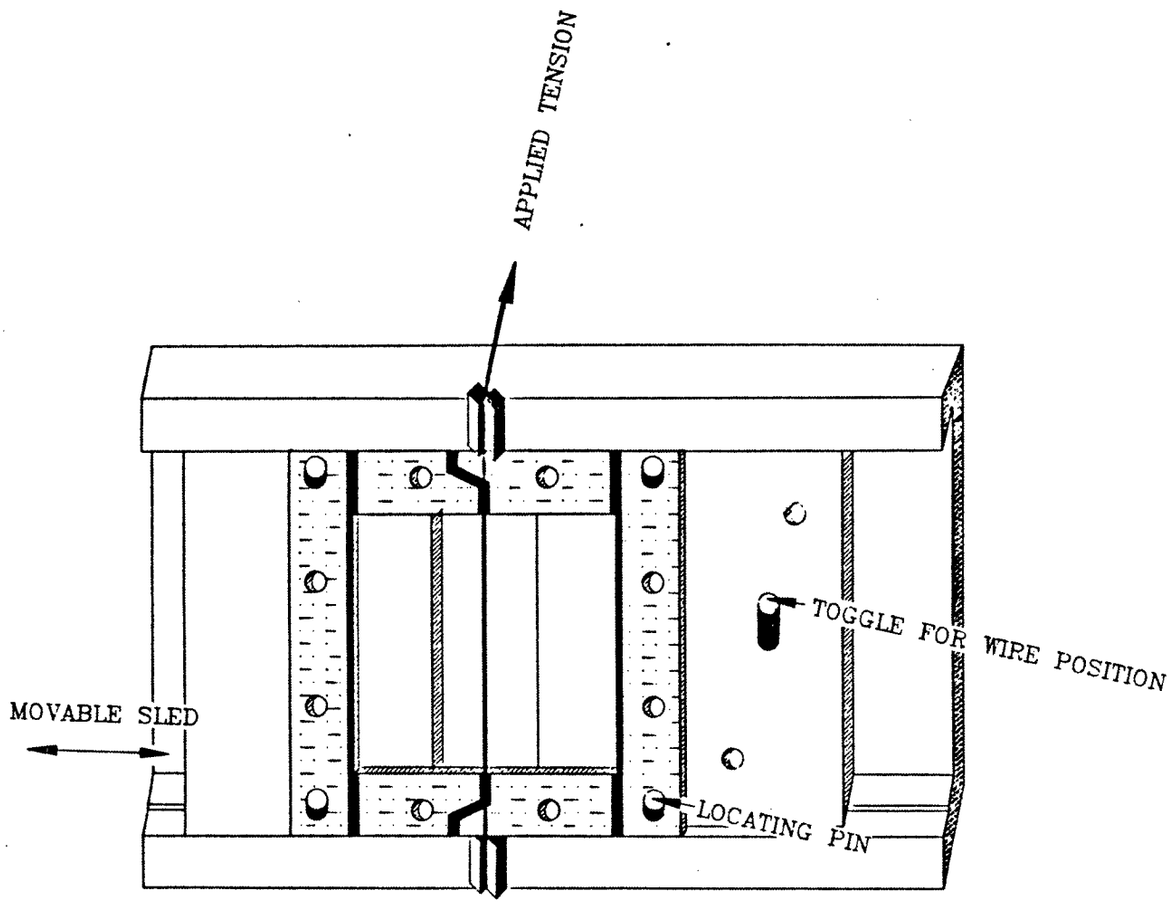

FIG IV.2

Stringing jig. Boards are positioned with 4 locating pins onto the sledge which moves laterally. Wire sits in the V-grooves. Three position toggle determines the wire position at centre or ±200 μm

the desired thickness of 0.5mm, rendering a cell depth of 4mm.

A modular type driftchamber is built starting with one type A wire cage board, followed by as many sequential driftcells as are desired and finished with another wirecage board. Nylon bolts are used on either end of the threaded rods to fasten the frames together. The finished chamber is very rigid, even if only three individual driftcells are used, which is the minimum of cells needed in order to solve the left-right ambiguity.

This method of assembly not only allows for an easy exchange of wire planes, but also the addition of extra drift cells for better resolution as well as the removal of cells if there are, for example, space limitatons. Wire planes can be pre-fabricated with any number of different wire diameters and/or wire materials. This permits not only fast replacement of a damaged wire, but also the complete exchange of specific wires with different ones which are more suited to a new task or another set of circumstances. The characteristic depth of some or all of the consecutive driftcells can be changed simply by installing a set of washers with appropriate thicknesses.

The assembled chamber was mounted inside a leak proof container with 0.5 mil thick Mylar windows. Gas tight feedthroughs have to be installed for the high voltages, the preamplifier bias voltage, the signals, and the drift gas flow tubes. Pictures of mounted MMDC's are shown in Fig V.2.

CHAPTER V. - MMDC VERSIONS BUILT FOR THE TRIUMF QQD SPECTROMETER

V.A. DESIGN CONSIDERATIONS

The specifications for the new chambers asked for high rate capability, high angular spatial resolution in the x-direction (width of the incident particle beam), and to a lesser degree angular resolution in the y-direction (height of the particle beam). Furthermore, the chambers should be run with the drift gas at atmospheric pressure. To achieve this, a compromise was necessary between high spatial resolution and high rate capability in the design of the drift cell. Two different systems were developed and tested. They are described in the following sections.

V.B. THE 8 WIRE MMDC

This system consisted of one single chamber, which in turn comprised eight consecutive drift cells, which were to measure particle trajectories in the x-z-plane. The third dimension y was to be determined via charge division read-out off the first and last wire.

The layout for this modular 8-wire drift chamber is shown in Fig. V.1. The dimension from cathode to cathode is 50 mm, i.e. the maximum drift distance is 25 mm. The anode wires are set off-centre alternatively by ±200μm in order to solve the left-right side

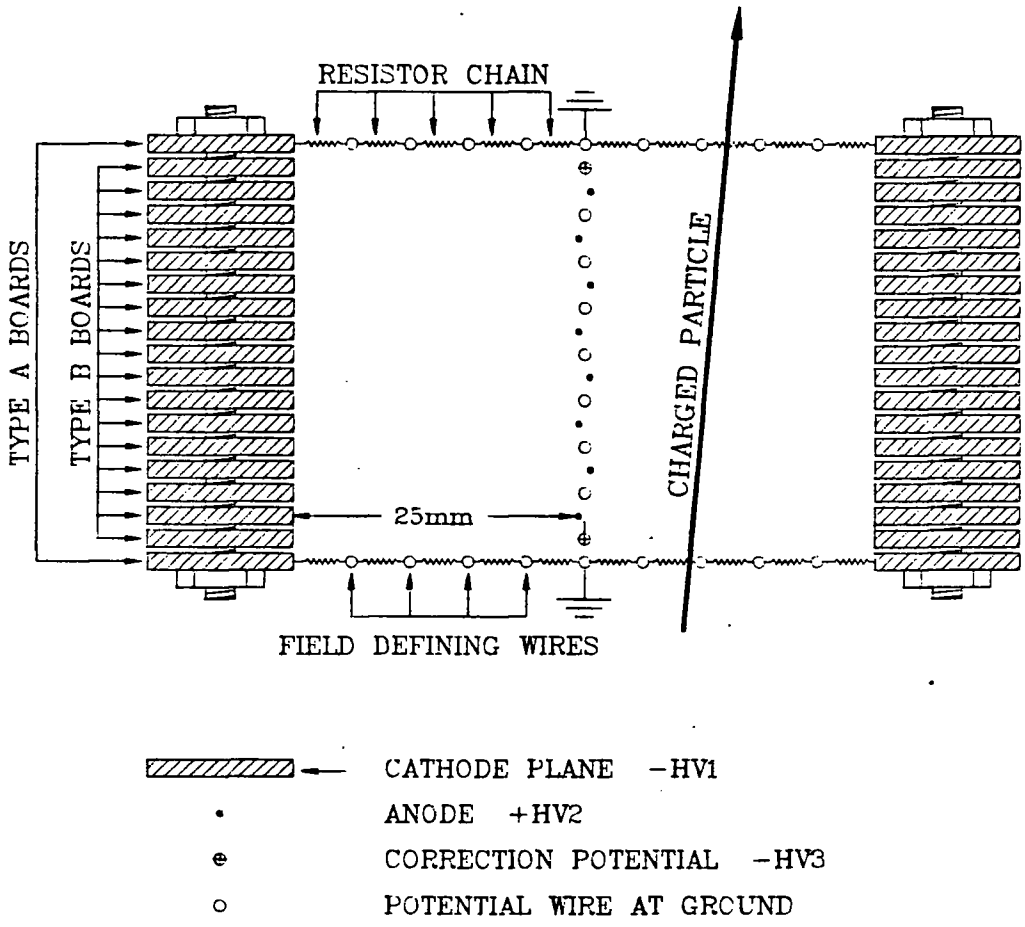

Fig. V.1

Modular 8-wire drift chamber. Max. drift distance is 25 mm. Anode wires are offset ±200 μm to resolve left/right ambiguity. Two field correction wires.

ambiguity. Two field correction wires are connected to a separate power supply. This provides the option of applying any independent voltage which may be required to correct field aberrations specific to the special position of the first and last drift cell in the chamber. The mounted MMDC8 is shown in Fig. V.2a.

The high voltages for the cathodes, the correction wires, and the anodes are fed through an RF choke. The electric signals are picked up directly form the pins on the boards and decoupled through 1000 pF capacitors. They pass through a preamplifier and then leave the gas container.

V.C. THE 4 WIRE MMDC

The second system which was built for the QQD spectrometer used three chambers. The trajectories in the xz-plane were given by the first and third chamber, each of which consisted of four drift cells (MMDC4). The less important y trajectory was measured only in the second chamber, the previously tested eight-wire model (MMDC8), which was rotated for this purpose by 90 degree with respect to the other chambers. Since there is no need for a charge division measurement in this three-chamber system, all anode wires were made from 20 μm thick gold-plated tungsten wire.

Fig. V.2b shows a mounted MMDC4. For this system, the feedthroughs are the same as described for the MMDC8. The gas container

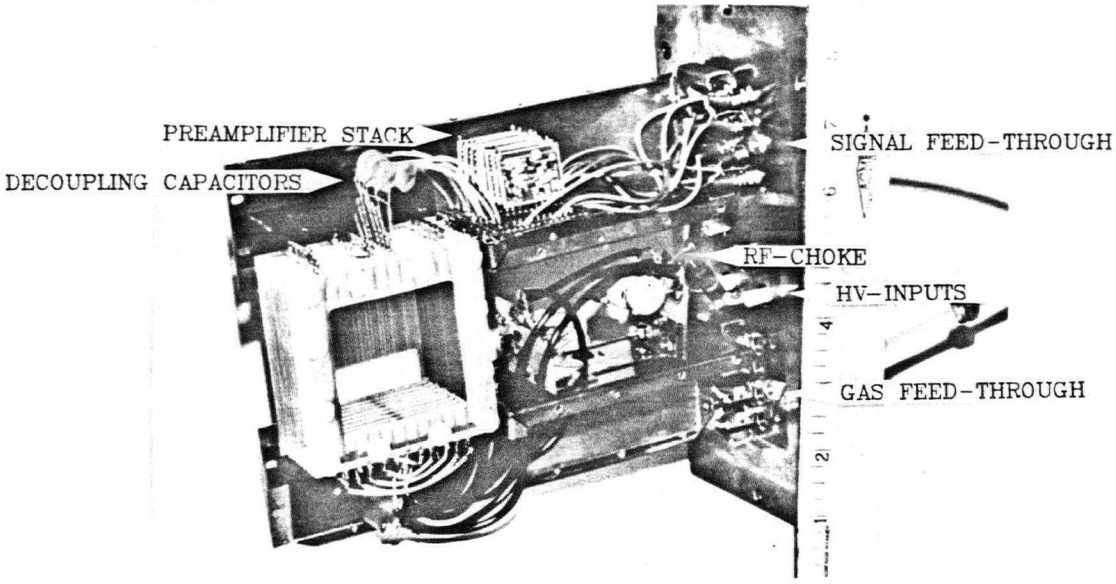

A

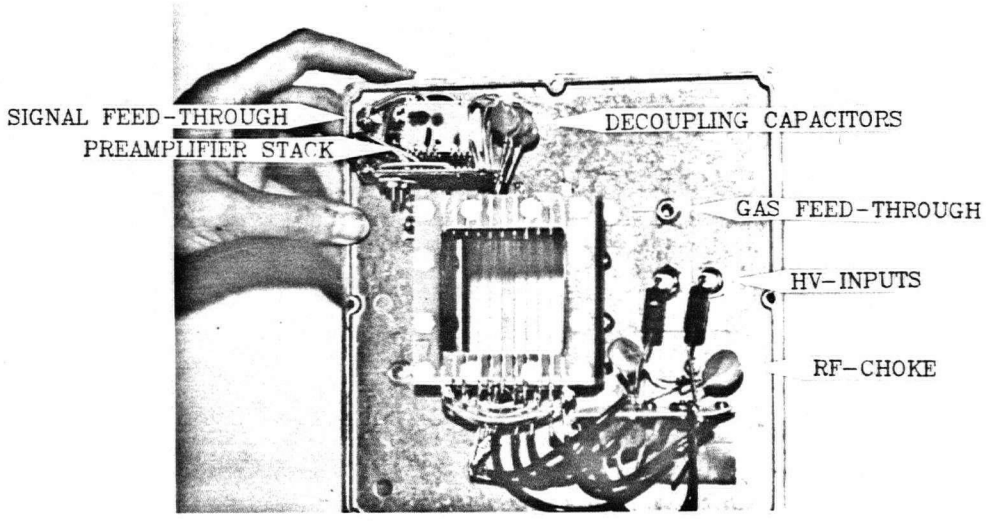

B

Fig. V.2

a) Mounted 8-wire chamber MMDC8

b) Mounted 4-wire chamber MMDC4

Copper shield for electronics is removed in both pictures

shown in Fig. V.2b was made specifically to hold one MMDC4. The other MMDC4 for this three-chamber system was simply mounted into the spare gas container used in the MMDC8 testing.

V.D. ELECTRONICS

The data acquisition block diagram is shown in Fig. V.3. The signals from each wire are fed through a 1000 nF decoupling capacitor into a fast rise-time (< 5 ns) hybrid preamplifier (see Fig. V.4 for a circuit diagram). Regular anodes are read out from one side only, anodes used for charge division measurements are read out from both sides. The signals are brought outside the gas container, where they are further amplified and discriminated in the "Eureocard" (see Fig. V.5). Both the "Eurocard" and the hybrid preamplifiers were fabricated in the TRIUMF electronics shop.

Out of the "Eurocard" comes a logic timing pulse for each wire. These pulses are fed through a twisted pair cable into the counting room, converted from ECL to NIM and provide the stop signals for an eight channel time to digital converter (TDC, LeCroy Model 2228).

For the charge division measurements, the analogue signals from top and bottom of each wire are transmitted in a similar way from the Eurocard via twisted pair cable directly to an analog to digital converter (ADC, LeCroy Model 2249A). A separate ADC unit was used for

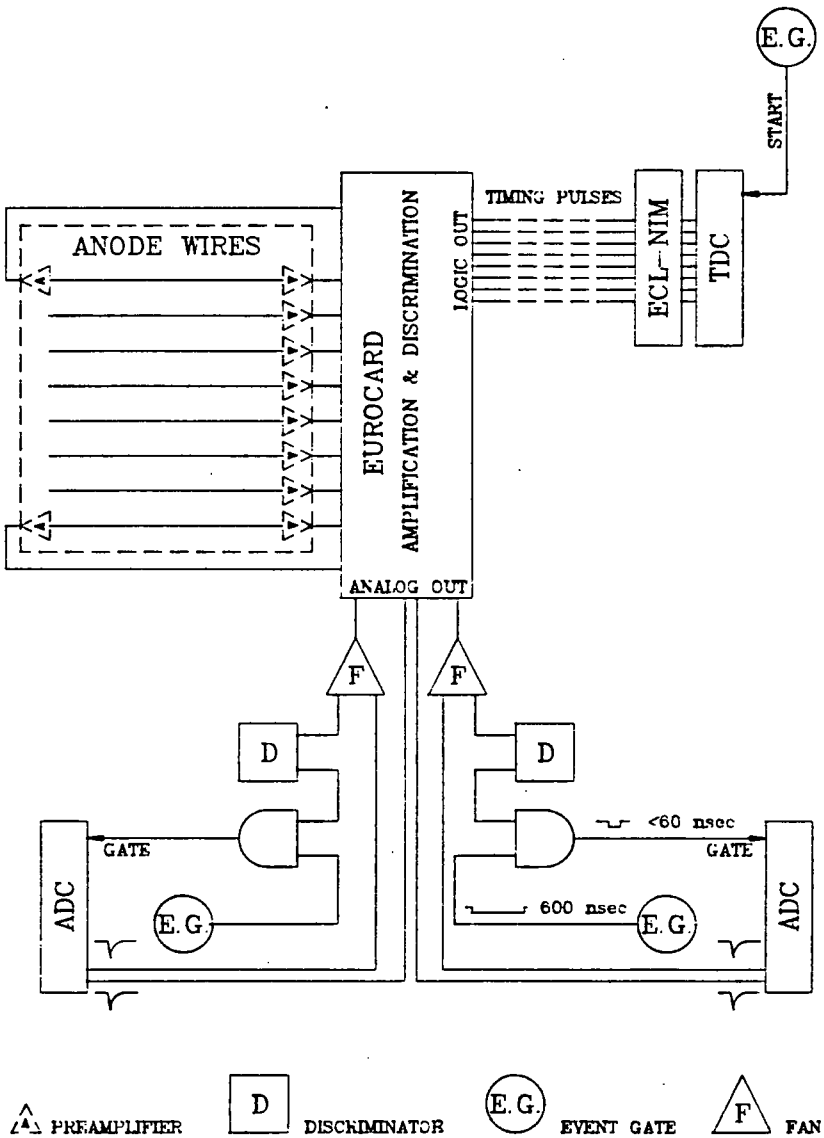

Fig. V.3

Electronics block diagram

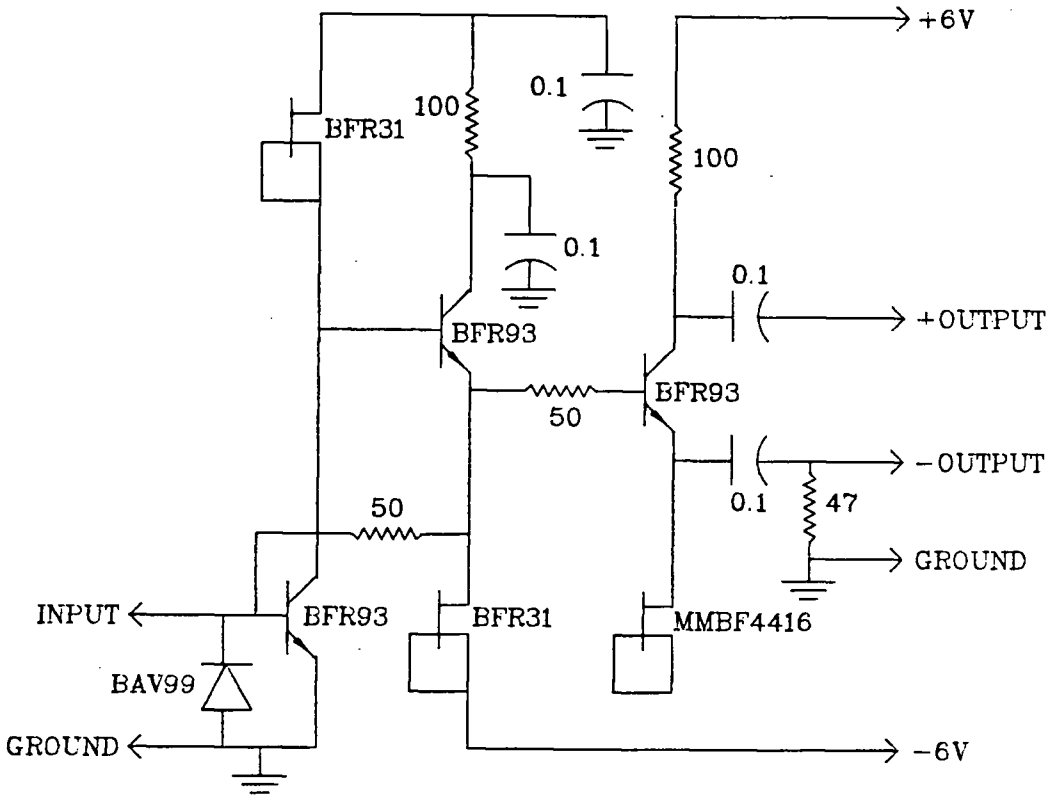

Fig. V.4

Preamplifier circuit diagram

All capacitors in units of μF

All resistors in units of Ω

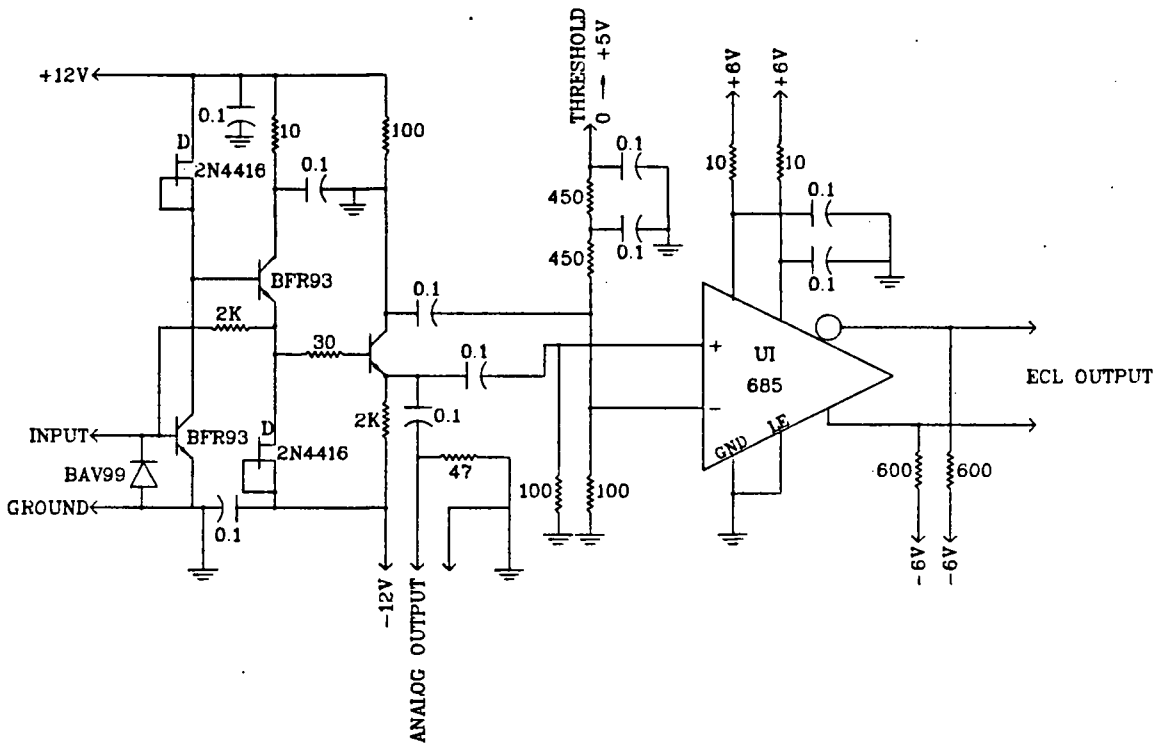

Fig. V.5

Eurocard circuit diagram

All capacitors in units of μF

All resistors in units of Ω

each wire. One of the two signals was fanned out, discriminated, and used in coincidence with the "event gate" signal as input gate for the ADC. The event gate is given by one discriminated scintillator output or the coincidence of the discriminated outputs of two scintillators for the bench testing. For the in-beam tests the "good event" strobe signal of the QQD spectrometer was used.

The ADC's and TDC's are read via CAMAC into the memory of a PDP-11 process computer and logged onto magnetic tape. The final data analysis was done on the TRIUMF VAX-cluster.

CHAPTER VI. - CALIBRATION SETUPS

VI.A. BENCH TESTING

VI.A.1. Laser velocity calibrations

The velocity calibration of a chamber includes not only the measurement of the drift velocity itself, but also the determination of the variation of this velocity throughout all areas of the detector.

Simulating tracks of ionizing particles with a pulsed laser gives the advantage of having a narrow, well collimated beam whose position can be defined with great accuracy. Laser calibrations have been the subject of much debate. The source of the ionization is a two photon absorption in some low ionization potential impurity in the chamber gas [17]. Such impurities are difficult to control since they could come from different sources such as the outgassing of materials from which the detector was constructed, pump oil vapour, or contaminated gas mixtures. This randomness of molecules available for ionization has lead to inconsistent data for different chambers, or even for the same chamber, tested at different times.

A pulsed N_2-Laser was used for this calibration which has a wavelength of 337nm ($h\nu$=3.68 eV). Ionization can occur whenever there are molecules present with an ionization potential $I < 2h\nu$ (< 7.36 eV).

In order to obtain a controlled and reproducible intensity of ionization, the chambers were doped with small quantities (~60 ppm) of N,N-diethylaniline $C_6H_5N(C_2H_5)_2$, which has an ionization potential of 6.99 eV. The gas induced ionization in the chamber is expected to build up as the concentration of the dopant increases with time. The build-up was exponential over the first five to ten minutes and levelled out after ~ 45 min, which is consistent with Ref. [17].

The setup for the laser calibrations of the QQD drift chambers is shown in Fig. VI.1. The laser beam was collimated with two quartz lenses and the beamspot cleaned up by a pinhole. A mirror, mounted on a micrometer transport (± 2μm) deflects the beam through the chamber. The chamber itself could be displaced vertically (±200 mm) on its stand.

An exposed plastic scintillator, mounted on a photomultiplier tube was used to trigger the electronic readout. During the tests the lights in the laboratory room were dimmed in order to protect the photomultiplier which was operating at a low Voltage (700V).

A typical raw TDC histogram for a single wire is shown in Fig. VI.2. Varying peak heights have no significance as the exposure time changed with each position. Fig. VI.3 shows TDC channel number versus laser beam position for the Argon(70%)-Isobutane(30%) drift gas mixture. The linearity of this plot demonstrates a constant drift velocity throughout the chamber.

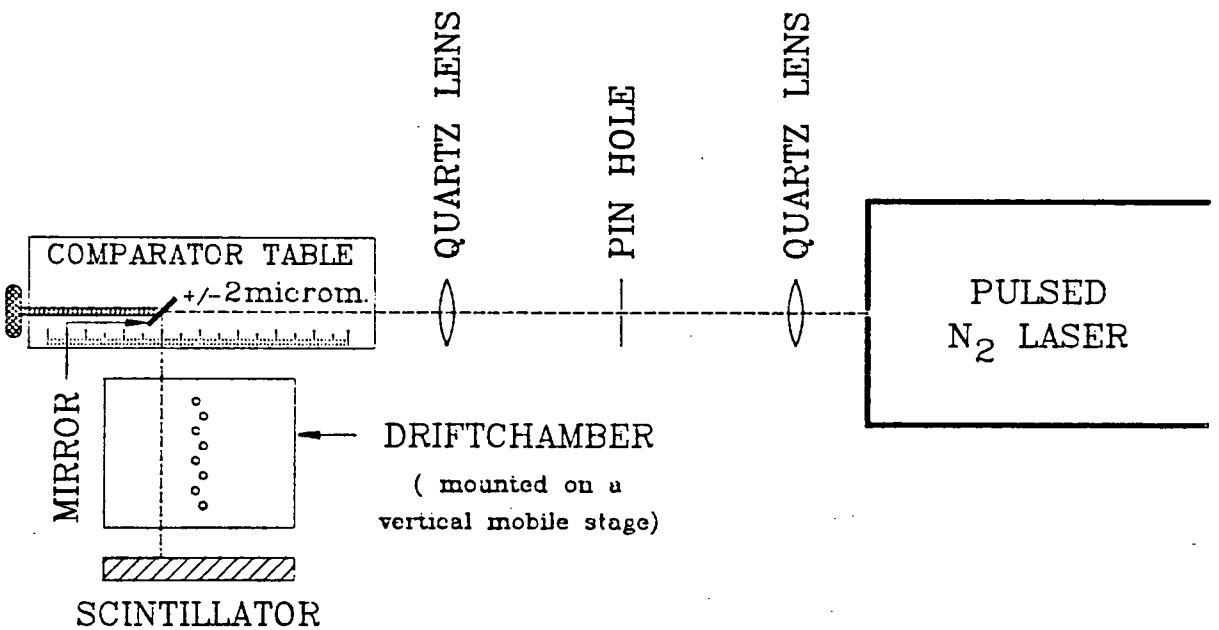

Fig. VI.1

Setup for laser calibration of drift velocity and efficiency

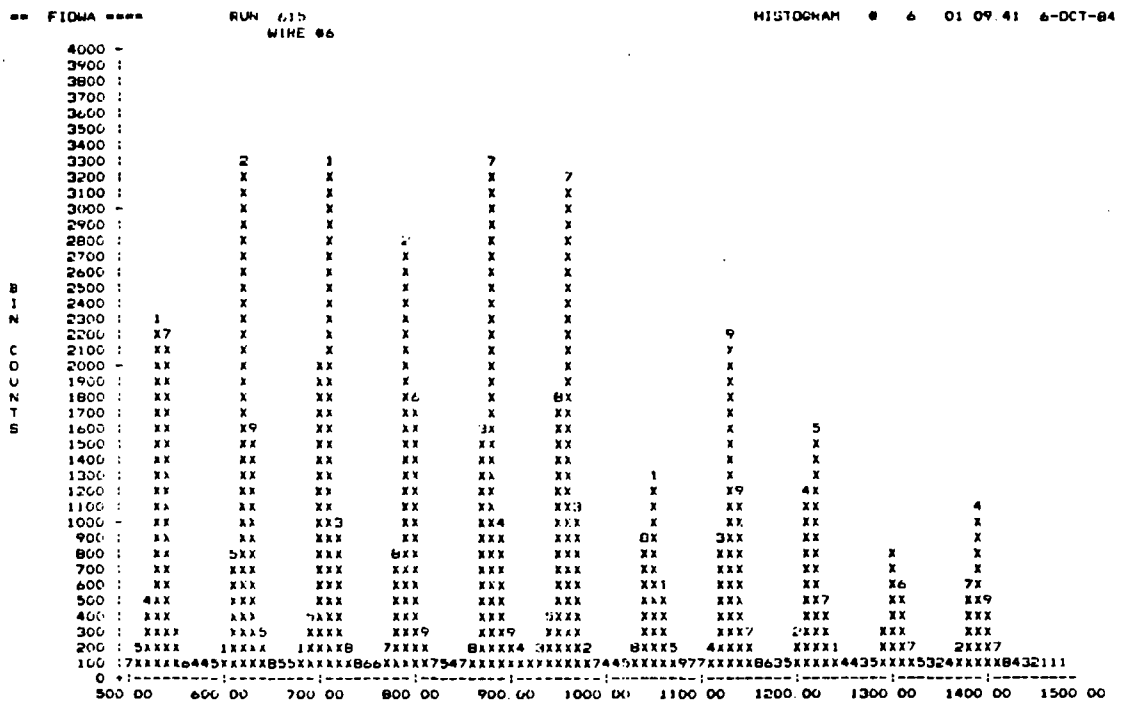

Fig. VI.2

Laser calibration of drift velocity (Example for wire #6 of MMDC8)

Peak separation corresponds to 2 mm shift of laser beam position.

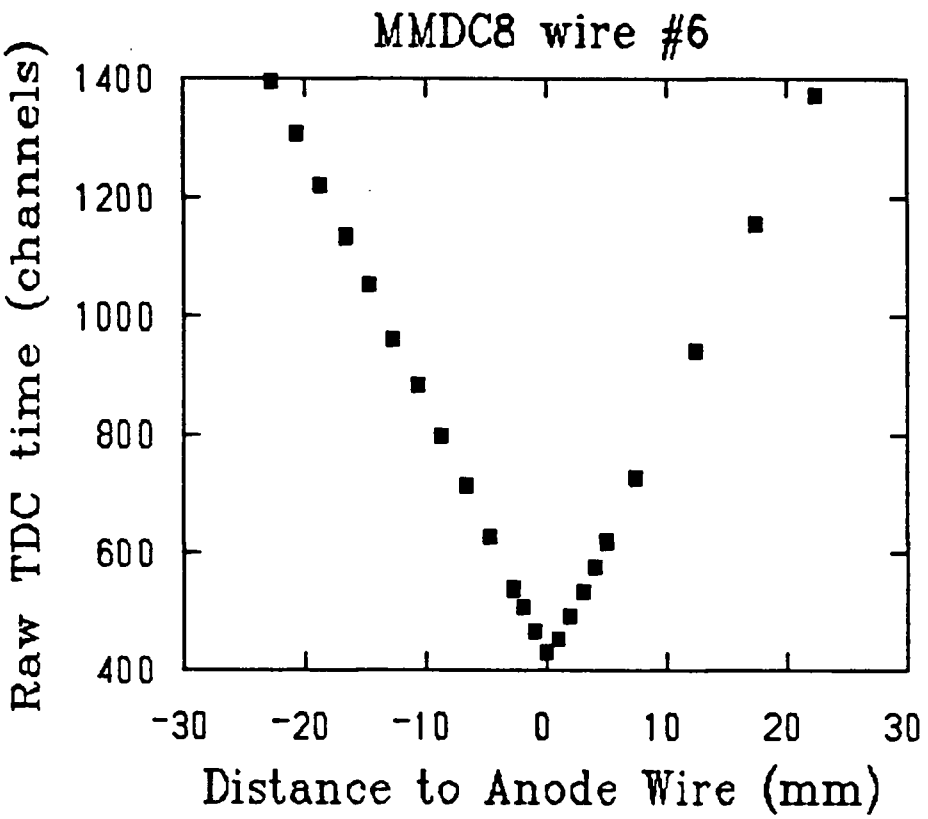

Fig. VI.3

Laser velocity calibration. Linearity demonstrates constant drift velocity throughout the chamber

The following observations were made concerning laser calibrations for drift chambers:

- No data should be taken within the first hour after doping.
- Direct contact between the laser beam and any wire should be avoided, since the photo-electrons ejected from the wire surface, will result in gigantic anode signals.
- For chambers which need windows thicker than 0.5mil, it will be necessary to replace the Kapton or Mylar window with a material which is transparent to UV radiation (i.e. Aclar).
- Chambers which require aluminized windows are not suitable for laser calibrations.

Due to the intrinsic width of the ionizing beam, laser calibrations cannot be used to find the true resolution of the detector. They are, however, a clean and fast method to determine the magnitude and uniformity of drift velocities throughout a chamber. The laser beam was easily collimated over large distances (50-100 cm), which allows several chambers to be tested and calibrated in coincidence.

A further advantage of laser calibrations is important if chambers are to be used in strong magnetic fields: As the laser light path, which liberates the drift electrons, is not affected by magnetic forces, the influence of any magnetic field on a drift chamber can be studied directly by using this method.

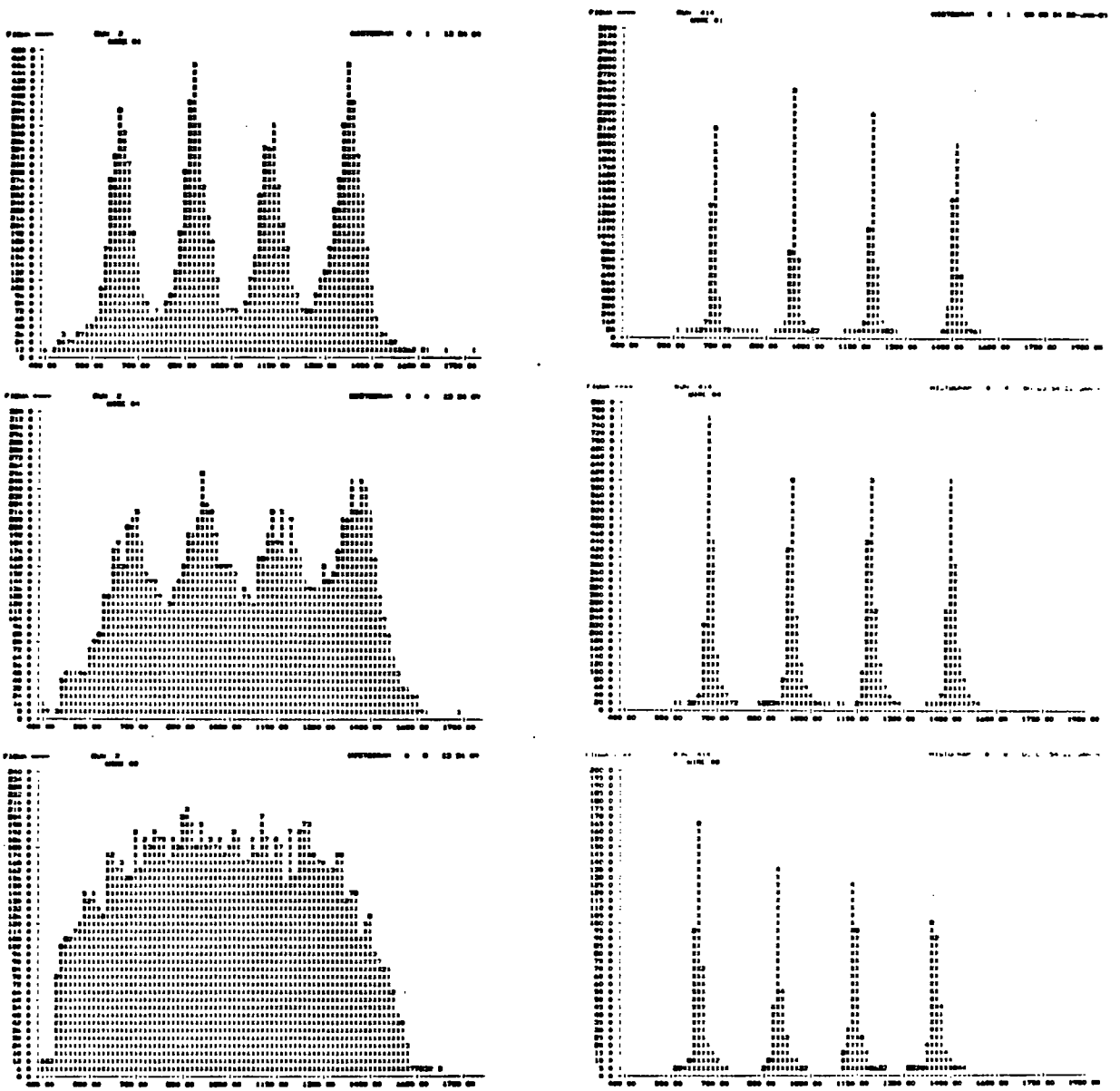

a) ^{106}Ru Source b)Laser

Fig. VI.4

Velocity calibration for MMDC8 (raw TDC histograms for wires #1,4,8) Neighbouring peaks in the histograms correspond to 5 mm shift of the calibrating beam. Deterioration of the spatial definition of the electron trajectory with increasing penetration into the chamber is clearly visible.

VI.A.2. β-Source Velocity Calibration

A further velocity calibration method was attempted using a source of the β emitter ^{106}Ru (100 μCi). The set-up from the laser testing (see Fig. VI.1) was used, with the collimated β-source in the place where the mirror had deflected the Laser beam through the chamber. In the sequence of Fig. VI.4, it can be seen that the β-beam is starting out well collimated. When it reaches wire #4, however, and even worse at the position of wire #8, its wide dispersion make it unsuitable for the calibration of multi-wire drift chambers.

VI.A.3. Laser Efficiency Tests for Wires

A graph which shows the efficiency of each wire as a function of the position of the ionizing track (Fig. VI.5) was made from the same data which were collected for the laser velocity calibration. The number of "triggers" received from the scintillator was compared to how many times each wire had fired. Since only one scintillator was used (the UV-laser beam was stopped in the plastic) rather than the coincidence of at least two, which would help to guard against noise triggering, the plotted efficiency results are only to be taken as lower limits.

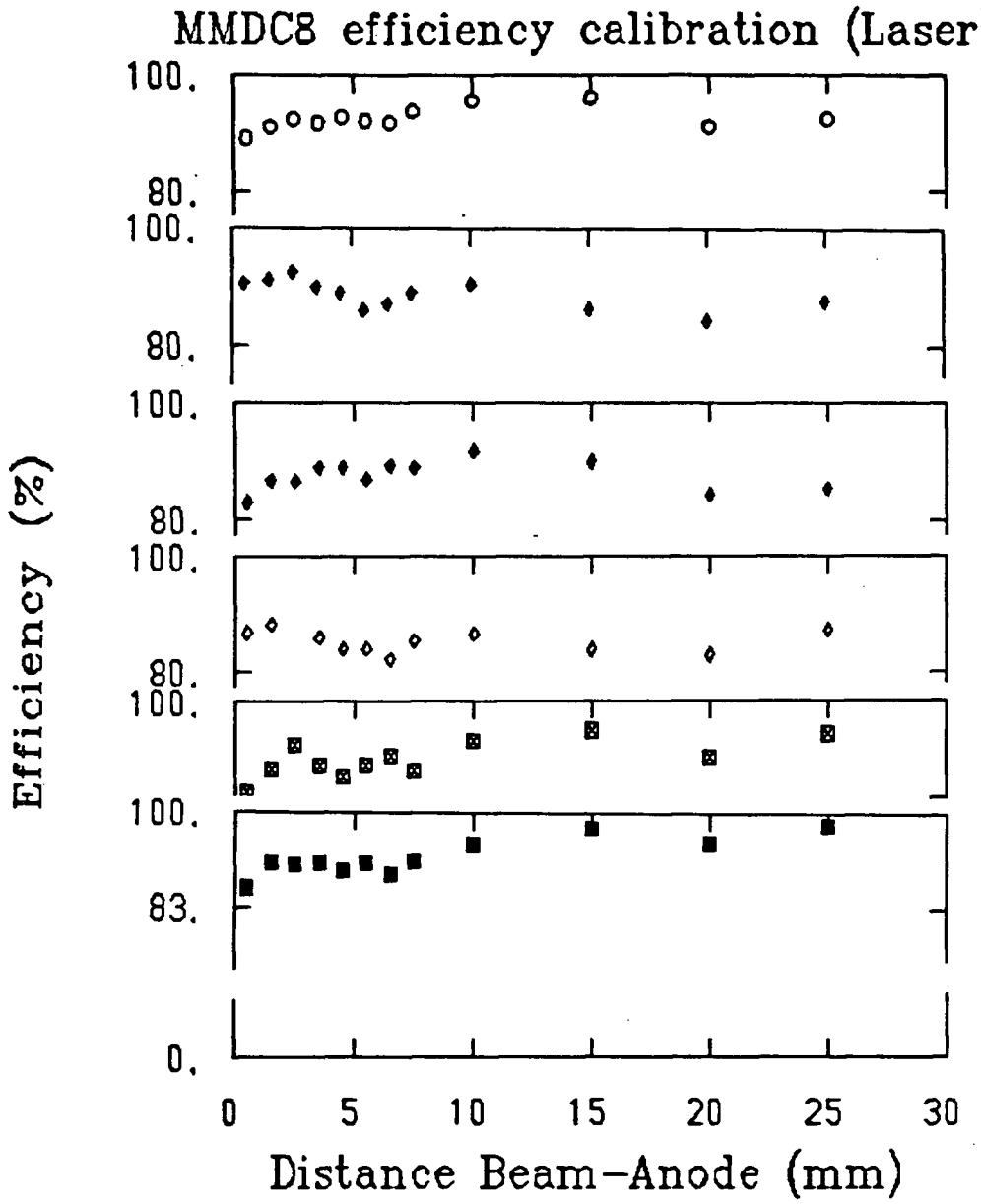

Fig. VI.5

Laser calibration: efficiency of the 6 central wires of MMDC8

VI.B. BEAM TESTING

VI.B.1. Velocity Calibrations

For the pion beam velocity calibrations, the MMDC8 was set up between two conventional MWPC's (see Fig. VI.6). The location of the pion in the drift chamber was calculated by projection, assuming a straight line trajectory through the two MWPC's space coordinates. For the purpose of testing all the drift space, i.e. the full width of the chamber, the beam had to be completely defocussed. In the scatterplot (Fig. VI.7) the traceback position in the drift chamber is plotted against the TDC channel number. There is a similar scatterplot from each wire, and again the linearity of the drift velocity extends throughout the chamber. For the purpose of calculating an exact drift velocity, very narrow calibration slits were defined at regular distance intervals. The resulting histograms were projected onto the TDC-axis, producing a peak for every calibration window. A straight line fit through all the calibration peaks was used for calculating the drift velocities.

VI.B.2. Multiplicity Test for Anodes

The MMDC8 was then mounted into the WC1 position (Fig. I.1) at the front of the QQD spectrometer. In order to determine the gas

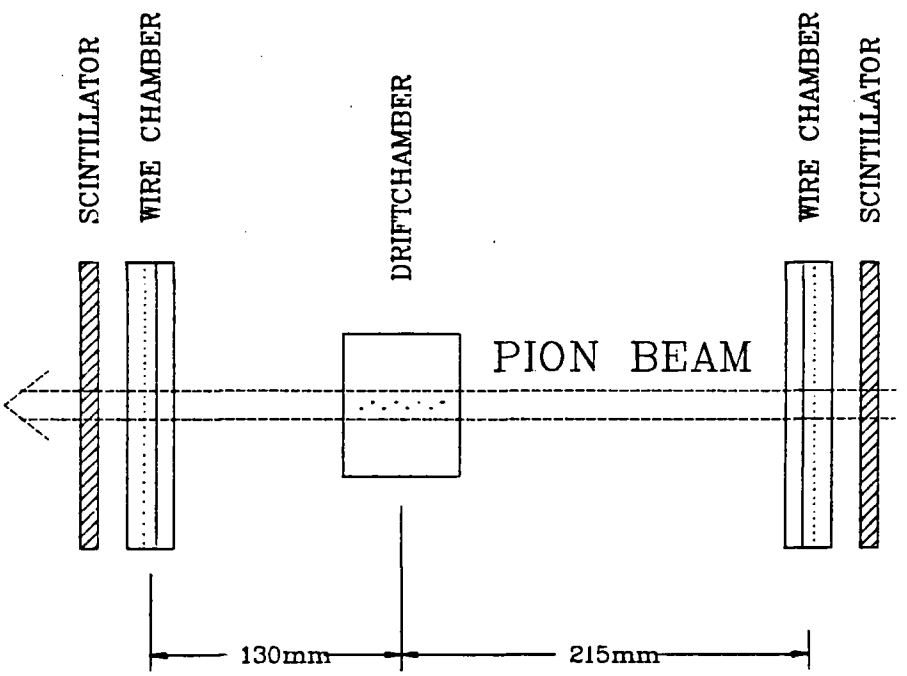

Fig. VI.6

Setup for "in beam" calibration of drift velocity.

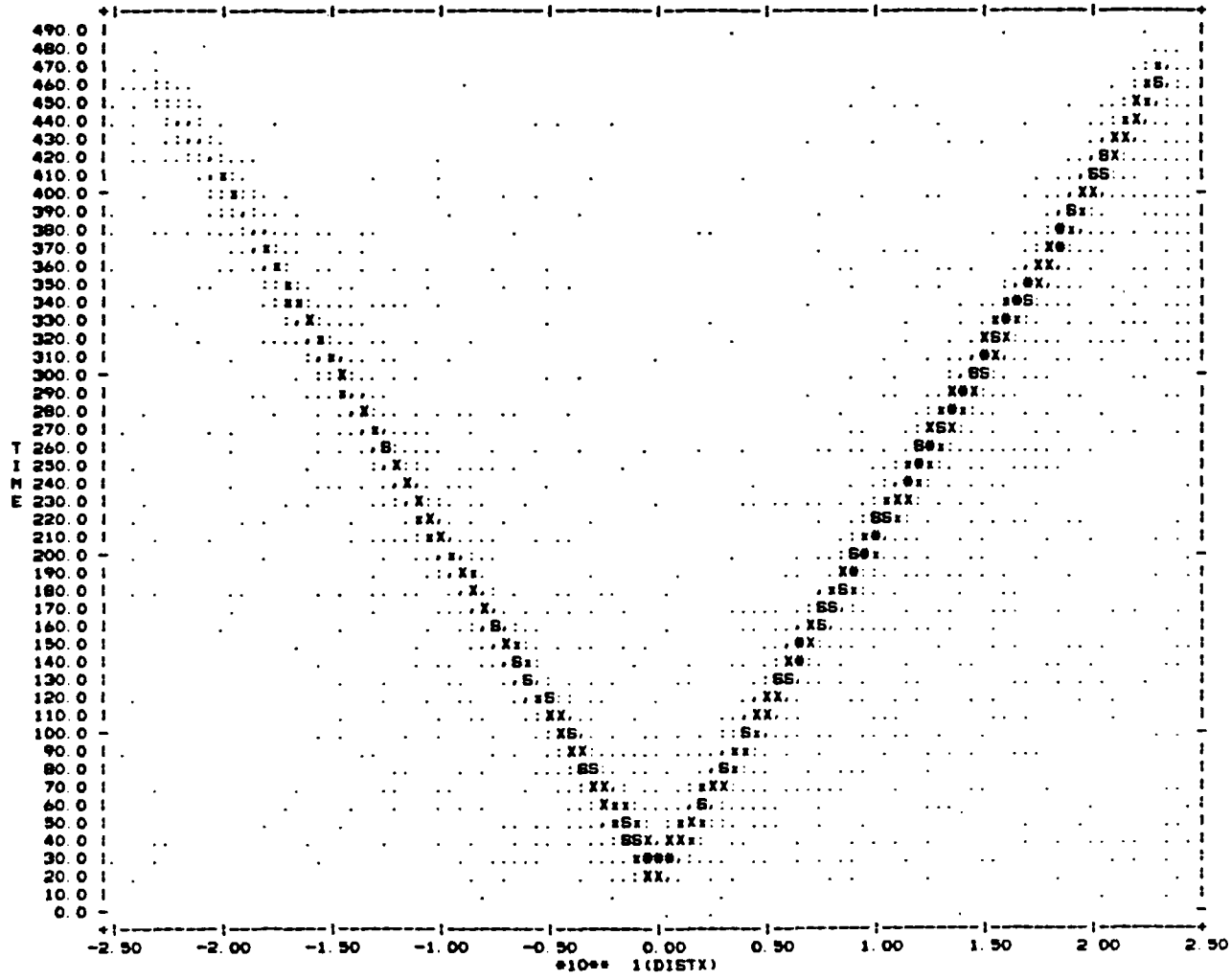

Fig. VI.7

Velocity calibration with wire chambers

gain needed for an efficient operation of the chamber, the multiplicity, that is the number of wires which had fired in response to a "good event" trigger, was monitored. A histogram of multiplicity versus the anode voltage is shown in Fig. VI.8.

VI.B.3. Data Taking for Resolution

Data has been taken with the MMDC8 chamber, when it was mounted in the WC1 position, as it was intended to be during experiments. At times the rate through the chamber was in excess of 10^6 particles/sec. The three chamber system was set up as shown in Fig. VI.9 for both the velocity calibrations and the data taking.

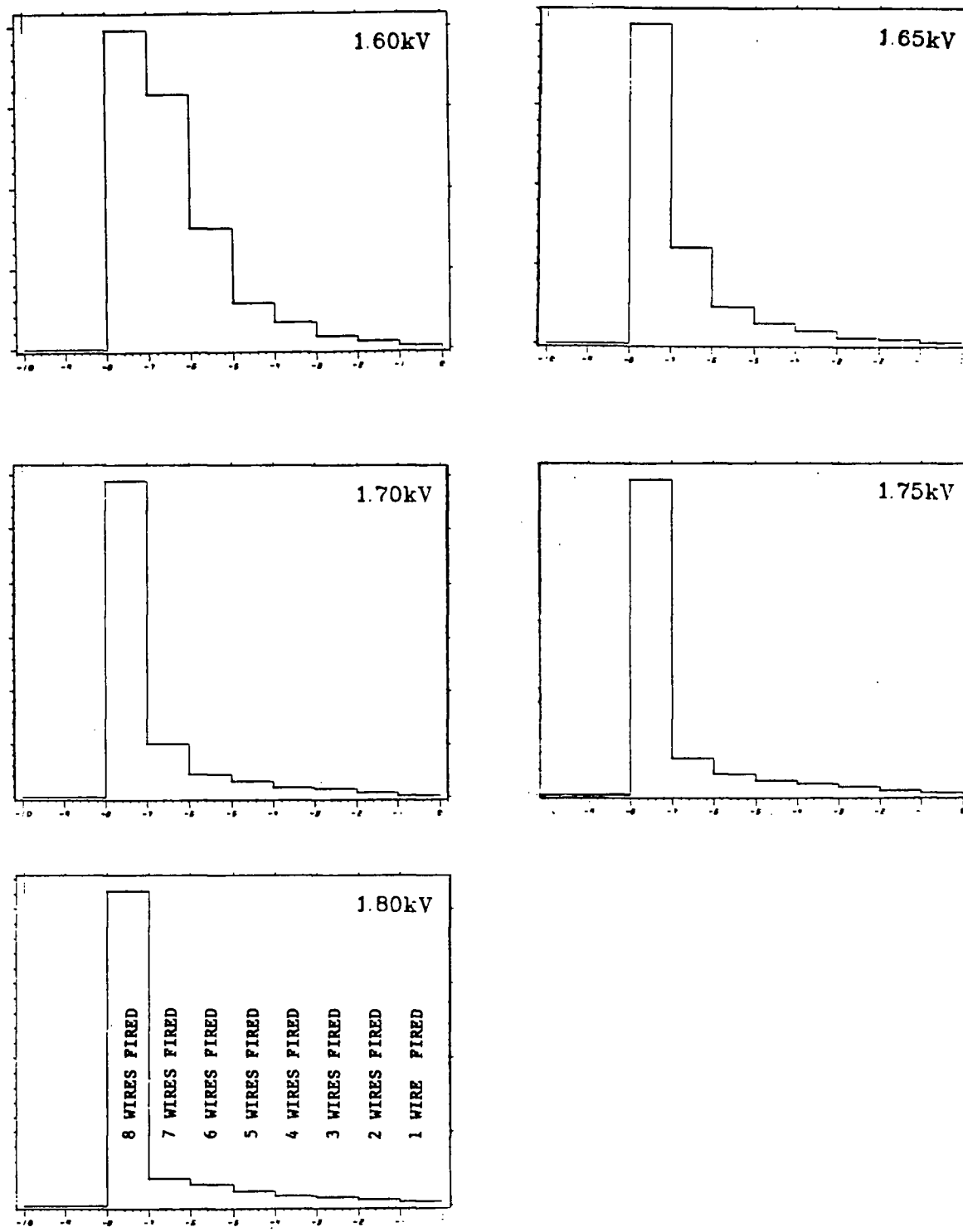

Fig. VI.8

Number of wires firing as a function of applied voltage

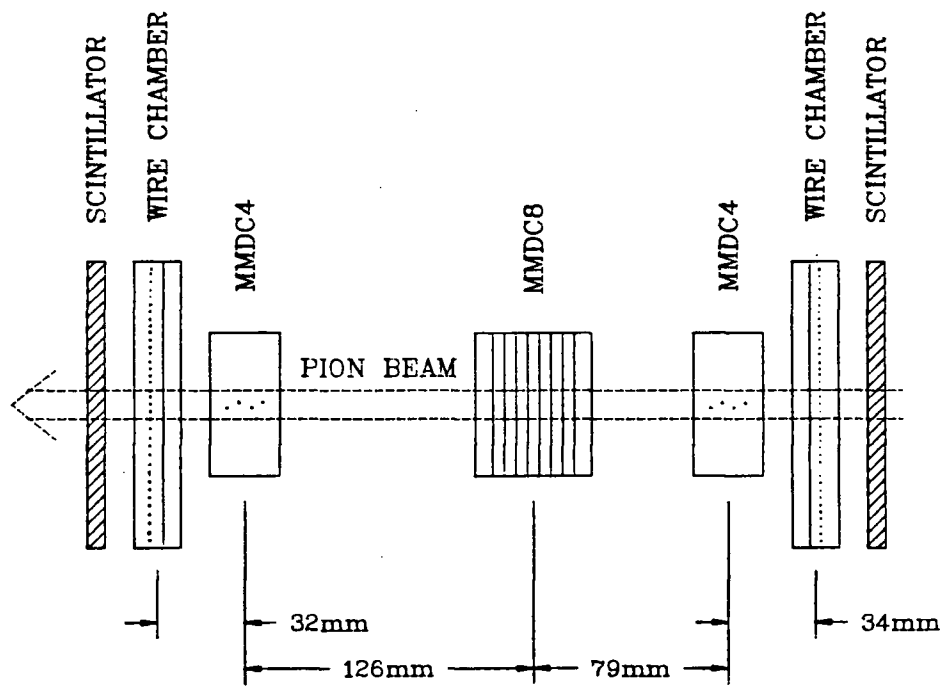

Fig. VI.9

Test setup for three-chamber system

CHAPTER VII. - DATA ANALYSIS AND RESULTS

When the measured drift times are to be converted into distances, the following points have to be considered:

Each TDC channel has a specific delay time and the position of each anode wire in the chamber is only known within mechanical tolerances. While the electronic delays certainly could be calibrated, the exact determination of any wire position is very difficult without having a detector available with at least similar or better spatial resolution than the chamber which is to be calibrated. Both the electronics delay times and the wire positions can be calculated, using a simple model for the chamber response.

The TDC data depend on two types of parameters:

a) Variables which vary from event to event, which are essentially due to track position and angle, and

b) Variables which are constant during a run, such as the wire offsets and TDC channel delays.

For each event, corrected times t'_{nk} with respect to the "type b)" parameters can be computed:

$$t'_{nk} = t_{nk} + TDC_k^{del} + \varepsilon_{nk} W_k^{off} \qquad \text{(VII.1)}$$

where t_{nk} is the raw TDC reading for wire number k, TDC_{nk}^{del} allows for

differences in delays in the electronics, W_k^{off} allows for the wire offset relative to the median plane of the anodes, and

$$\varepsilon_{n\,k} \text{ is } \begin{cases} +1 & \text{if the track is to the left} \\ -1 & \text{if the track is to the right} \end{cases}$$

This implies that $\varepsilon_{nk+1} = - \varepsilon_{nk}$.

The following is a step by step description of how the correction coefficients TDC_k^{del} and W_k^{off} were determined for the 6 inner wires of the MMDC8. The data set was restricted to events where all six wires had fired. The left-right ambiguity was resolved by first assuming that all particle trajectories were in the left half of the chamber. Then a least squares fit for the trajectory to the data points (raw TDC values) was calculated. Due to the ±200 μm wire offsets, the chi-square values for the tracks which actually did go through the left half of the chamber were much lower than the values for the right half. Fig. VII.1 shows that events can be clearly separated by this method. A similar histogram is obtained by assuming that all tracks went through the right half of the chamber.

Assuming no wire offset, the particle track can be described by position and angle parameters $\tau_{3.5n}$, $\tau_{\Delta n}$. The centre of the chamber was chosen as reference in order to make the error matrix diagonal.

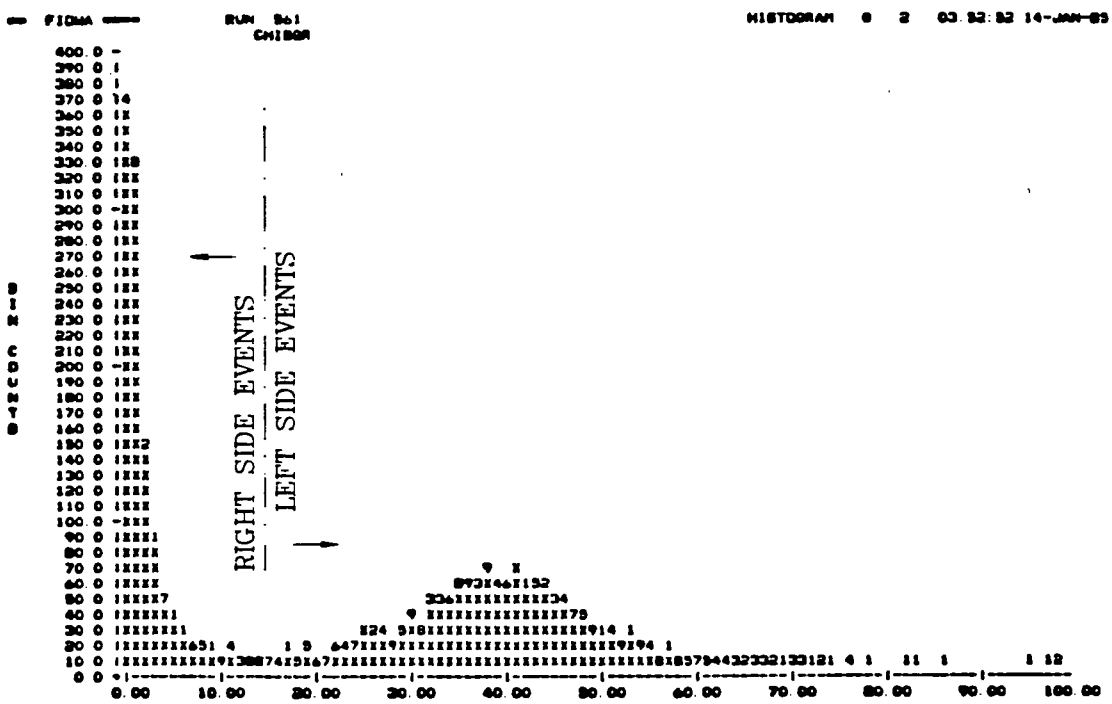

Fig. VII.1

Track fitting: Chisquare distribution obtained assuming all trajectories in right half of chamber. Similar histogram is obtained if all trajectories are assumed in left half of chamber.

Then the corrected time t'_{nk} is given by

$$t'_{nk} = \tau_{3.5n} + (k - 3.5)\tau_{\Delta n} \qquad \text{(VII.2)}$$

The correction coefficients TDC_k^{del} and W_k^{off} can now be determined by the maximum likelihood method (see Appendix).

During the first pass through the data, compute the corrected times t'_{nk}. $TDC_{k_o}^{del}$ can be set to zero and the initial guesses for $W_{k_o}^{off}$ can be the same for each wire. A least squares fit is made to determine the track position and angle. The 2x2 normal matrix is computed, where the data set are the six t'_{nk} and the variables are $\tau_{3.5}$ and $\tau_{\Delta n}$, the diagonal terms are the squares of uncertainties in $\tau_{3.5}$ and $\tau_{\Delta n}$. Now the least square value χ^2 for the event can be calculated. If σ_k is the position resolution (in unit of drift times), then

$$\chi^2 = \sum_{k=1}^{6} (t'_{kn} - \tau_{3.5} - (k-3.5)\tau_{\Delta n})^2 / \sigma_k^2 = \sum_{k=1}^{6} (\Delta_{kn}/\sigma_k)^2 \qquad \text{(VII.3)}$$

The initial guess for σ_k can be common to all wires. χ^2 is binned into a common histogram, as well as accumulated separately for each wire. The contribution from this event to the 2x2 error matrix for each wire can be calculated. The inverted error matrix is used to find corrections to TDC_k^{del} and W_k^{off} at the end of this pass, i.e. c_k^{del} and

c_k^{off} are determined such that

$$\sum_n \left(\frac{\Delta_{nk} - c_k^{del} - \epsilon_k c_k^{off}}{\sigma_k}\right)^2 \qquad \text{(VII.4)}$$

(summed over all events), is a minimum.

At the end of the pass σ_o is multiplied by $\sqrt{\chi^2/N}$ (where N is the number of degrees of freedom, in this case N=4n), in order to get a new estimate for the resolution per wire for the next pass.

Also make the substitutions:

$$TDC_k^{del} + c_k^{del} \Longrightarrow TDC_k^{del} \qquad \text{and}$$

$$W_k^{off} + c_k^{off} \Longrightarrow W_k^{off} \qquad \text{for use with the next pass.}$$

It was found that only 2 to 3 passes were needed to find the correction coefficients. As shown in Table I, only very few events have to be analyzed to give reliable coefficients. Fig. VII.2 shows the chisquare distribution for all six wires after the first pass (without any TDC corrections). The second column shows the chisquare distribution for each wire with the final TDC coefficients.

TABLE I

TDC Correction Coefficients

# of Events analyzed	correction to individual wires (units: TDC channels)					
	#1	#2	#3	#4	#5	#6
375	-18.97	14.53	16.63	1.72	-16.60	2.69
3648	-19.00	14.03	17.16	1.73	-16.06	2.14
18547	-18.94	14.36	16.55	1.91	-16.18	2.31

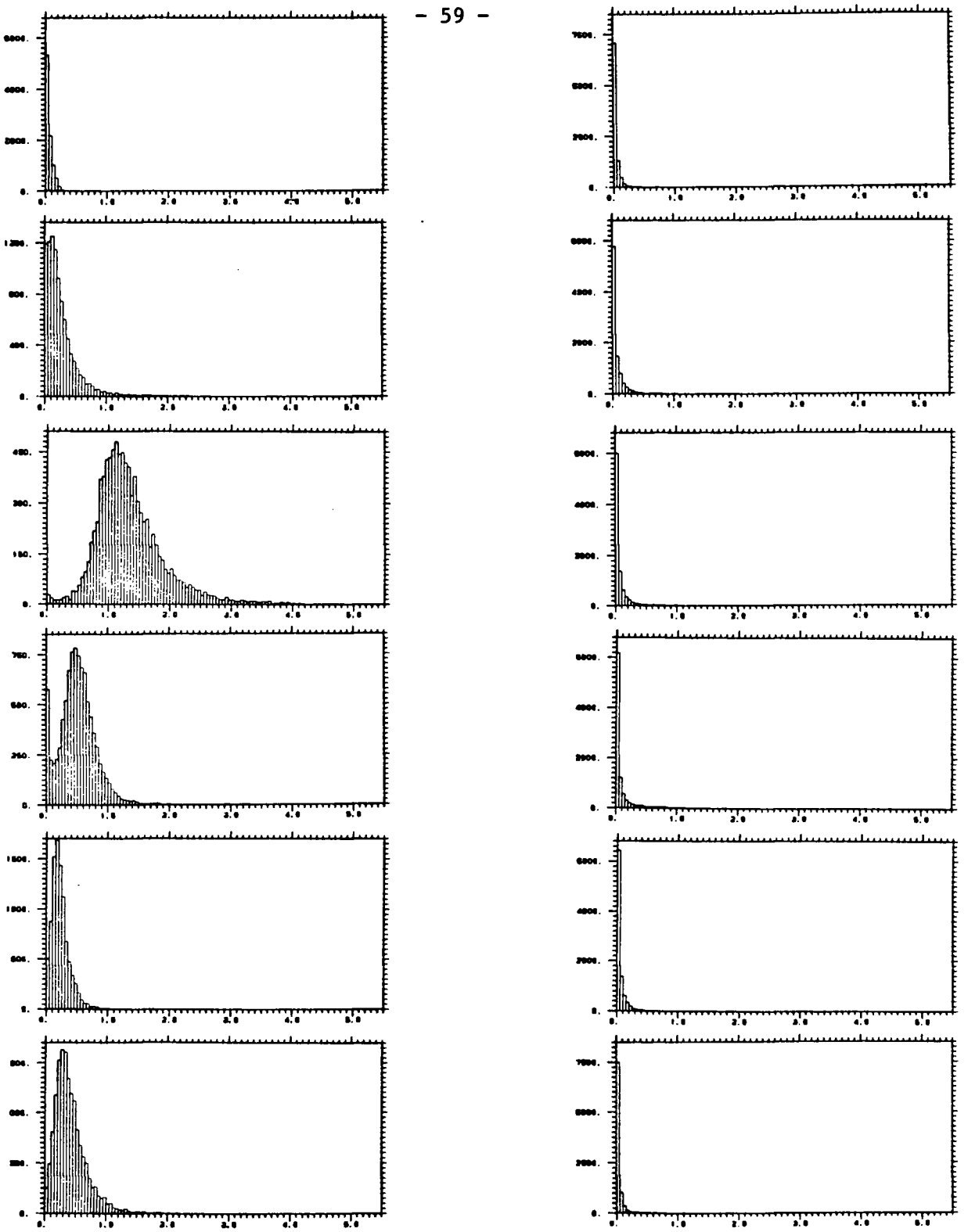

after first pass of analysis

with final TDC coefficients

Fig. VII.2

Chisquare distribution for all six wires of MMDC8.

TABLE II

Resolution of the Eight Wire Chamber

(MMDC8 6 wires considered)

GAS	VELOCITY (μm/nsec)	σ(mean) (μm)	ANGULAR (mrads)	TARGET FWHM(mm)
I	51.8	145±1	17.1±.1	3.59
II	51.9	114±1	13.4±.1	2.81
III	40.9	77.4±.2	9.11±.02	1.91
IV	54.8	151±1	17.8±.1	3.74
V	60.8	143±1	16.8±.1	3.53
VI	64.4	126±1	14.8±.1	3.11

Key to the gas mixtures:

I ARGON 80% - METHANE 20% (PREMIX)

II ARGON 50% - ETHANE 50% (PREMIX)

III ARGON 50% - ETHANE 50% (IN HELIUM)*

IV NEON 80% - ETHANE 20%

V NEON 65% - ETHANE 35%

VI NEON 50% - ETHANE 50%

*Helium from the spectrometer leaked through Mylar window into the chamber.

TABLE III

Resolution with Changing Drift Field

(MMDC8 6 wires considered)

FIELD (KV/cm)	σ(mean) (μm)	σ(wire #2) (μm)	ANGULAR (mrads)	TARGET (mm) FWHM
1.20	119.0±1.4	160.4±4.4	14.0±.2	2.94
1.40	113.7±0.6	148.8±1.9	13.4±.1	2.81
1.60	115.2±0.9	153.8±2.8	13.5±.2	2.84

(AR 50% - ETH 50%) PREMIX

TABLE IV

Resolution with Changing Gas Gain

(MMDC8 6 wires considered)

ANODE (KV)	σ(mean) (μm)	σ(wire #2) (μm)	ANGULAR mrads)	TARGET (mm) FWHM
1.90	113.9±0.5	148.0±1.7	13.4±.1	2.81
1.85	114.0±1.6	150.8±5.2	13.4±.2	2.81
1.80	113.7±0.6	148.8±1.9	13.4±.1	2.81
1.75	113.7±1.8	155.7±5.7	13.4±.2	2.81
1.70	116.0±1.6	166.6±5.6	13.6±.2	2.86

(AR 50% - ETH 50%) PREMIX

TABLE V

Resolution of the Four Wire Chamber

(MMDC4 4 wires considered)

GAS	VELOCITY (μm/nsec)	σ(mean) (μm)	ANGULAR (mrads)
I	68.9	138.1±1.2	27.1±.2
II	43.2	104.6±0.8	20.5±.2
III	66.8	124.5±1.2	24.4±.2
IV	67.6	130.0±0.9	25.5±.2

Key to the gasmixtures:

I (ARGON + METHYLAL)* 70% - ISOBUTANE 30%

II ARGON 80% - ETHANE 20%

III (ARGON + METHYLAL)* 80% - ETHANE 20%

IV (ARGON + METHYLAL)* 50% - ETHANE 50%

*The Argon was bubbled through liquid Methylal wich was kept at 0° C. Estimated Methylal content ~(3-4)% of Argon content.

TABLE VI

THE HORIZONTAL ANGULAR RESOLUTION IN THE THREE CHAMBER SYSTEM

(2 MMDC4 positioned 200mm apart)

GAS	ANGULAR (mrads)	TARGET FWHM (mm)
I	1.63	0.34
II	1.29	0.26
III	1.47	0.31
IV	1.53	0.32

Key to the gasmixtures:

I (ARGON + METHYLAL)* 70% - ISOBUTANE 30%

II ARGON 80% - ETHANE 20%

III (ARGON + METHYLAL)* 80% - ETHANE 20%

IV (ARGON + METHYLAL)* 50% - ETHANE 50%

*The Argon was bubbled through liquid Methylal which was kept at 0° C. Estimated Methylal content is ~(3-4)% of Argon content

To convert the TDC channels into actual drift distances and resolutions of wires, the calibrated drift velocities were needed. All TDC measurements were done with the same unit (LeCroy Mod. 2228). Its time range was extended to 740 nsec to allow electrons to drift the full 25 mm maximum distance even in very slow gas mixtures. This TDC unit was then calibrated and found to measure 0.38 nsec/channel.

The results of the beam tests, done with 50 MeV/c pions, are summarized in the following tables:

Table II shows the resolution of the eight wire MMDC with different gas mixtures. Only the six inner wires were considered. The high resistance wires in the first and last positions did not give consistent responses, due mostly to electric field aberrations (see below). Most significant is the improvement in the resolution due to the addition of Helium to the Argon-Ethane mixture.

Table III shows the resolution for the same chamber with different electric fields, while Table IV summarizes how the resolution changes with changes in the gas gain, i.e. different anode voltages.

The test results for the four wire MMDC are shown in Table V. while the horizontal resolution of the three chamber system tests are listed in Table VI. The vertical dimension was determined by the previously tested 8-wire MMDC which was rotated by 90 degrees for this purpose. Therefore the vertical resolution for the three chamber system is also contained in Table II.

The results for the charge division measurements are shown in Fig. VII.4. The resolution is approximately 2 mm. As seen in the map of the equipotential lines for the MMDC8 (Fig. VII.5a), both wires used for the charge division read-out (in cell #1 and cell #8) are not very efficient for particles passing more than 10 mm away from the anode. On the other hand, the applied correction voltage was not able to correct the field near the anode (Fig. VII.5b). So for tracks close to the centre of the chamber, the first and last drift cell had an effective cell depth of 6mm, which is much more than the 4 mm standard depth for all other cells. It follows that the resolution in the first and last cell is worse.

All the chambers have been running with incoming pion rates in excess of 10^6 particles/sec.

Testing of the chambers has been severely limited by frequent break-downs of the newly developed preamplifiers and amplifier - discriminators. The sense wires were damaged during the testing, when a premixed drift gas was found to be heavily contaminated with propene. In Fig. VII.6 the magnified wire surface is shown.

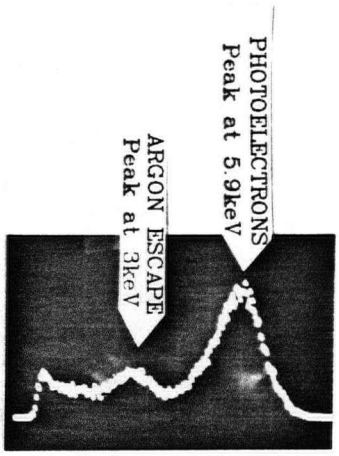

a) Pulse height spectrum of ^{55}Fe

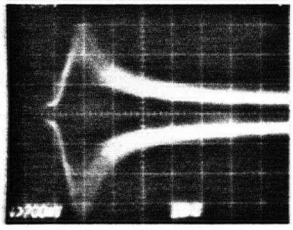

b) Oscilloscope signals from both ends of anode wire (top signal inverted, source at centre of wire)

c.1) y=+20mm

c.2) y=+10mm

c.3) y= 0mm

c.4) y=-10mm

c.5) y=-20mm

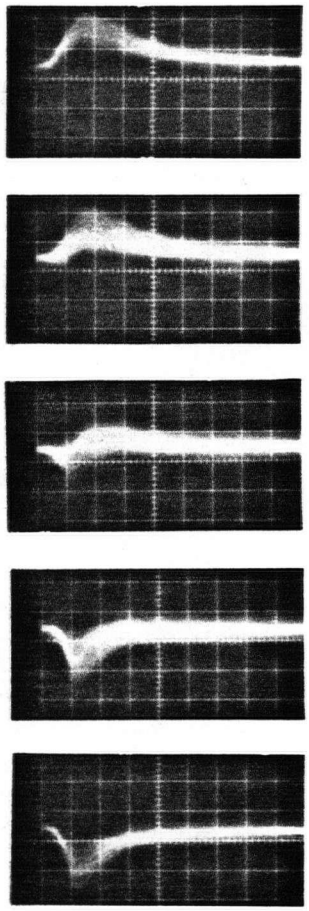

c) Difference of signals from b) for different y-positions of the ^{55}Fe source.
Vertical: 100mV/div.
Horizontal: 10nsec/div.

Fig. VII.3
Charge division method with ^{55}Fe source

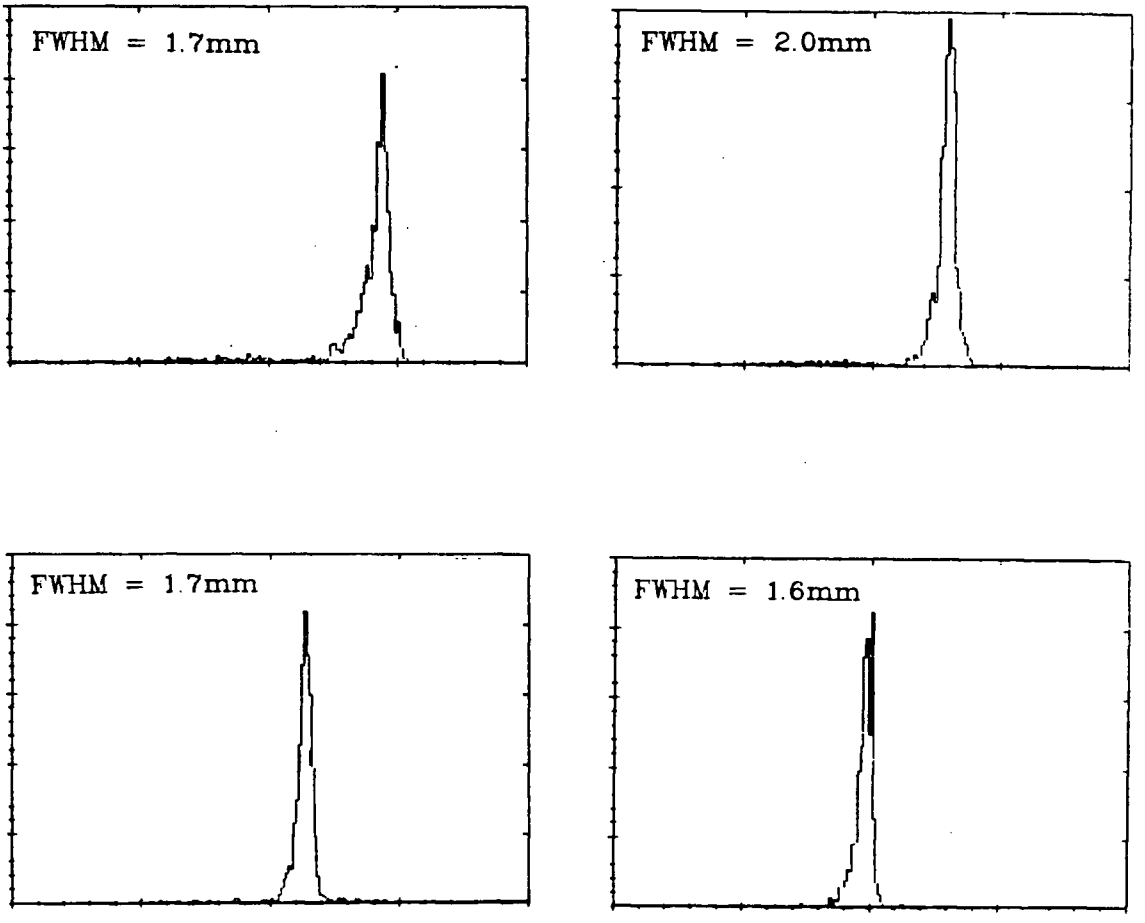

Fig. VII.4

Laser calibration of y-resolution with the charge division method. Peak shifts correspond to 5 mm.

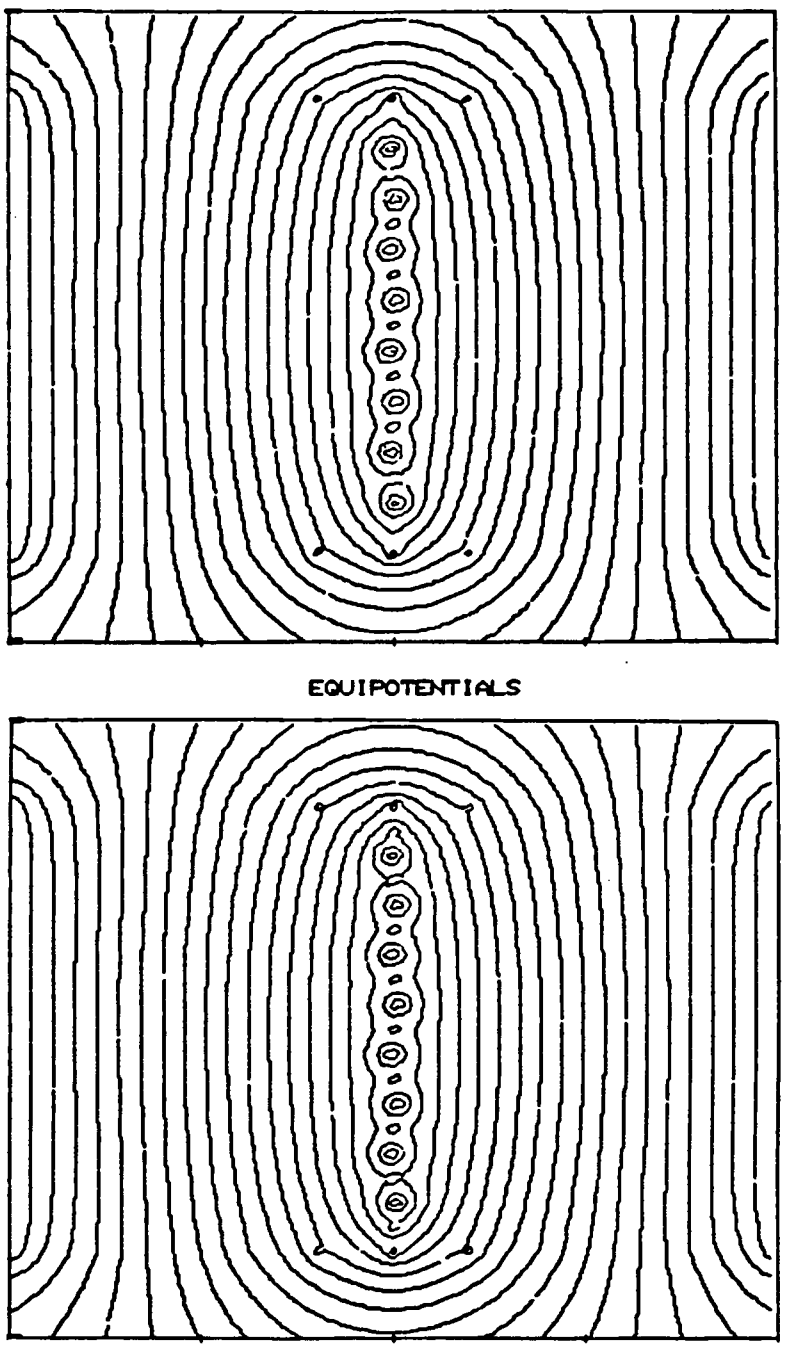

Fig. VII.5

Calculated field maps for MMDC8

a) without correction voltage

b) with correction voltage of 300 V.

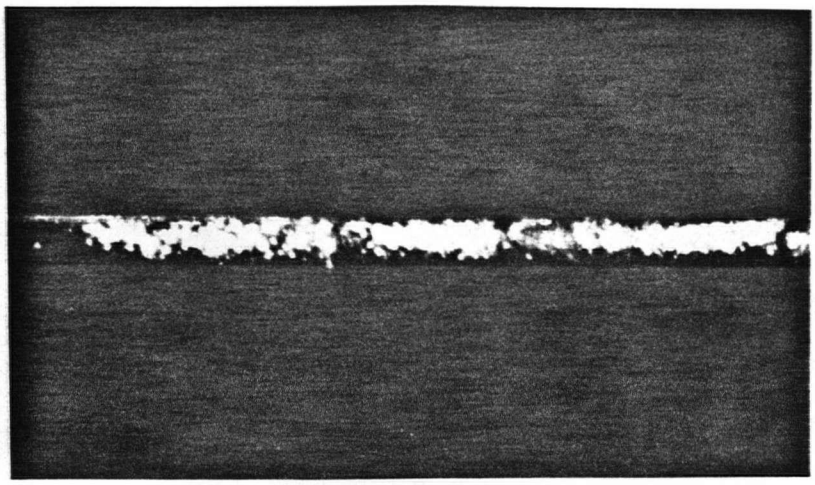

A

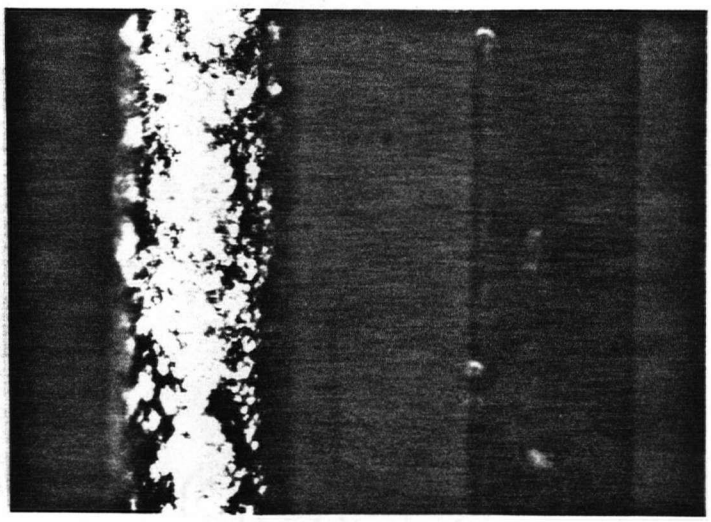

B

Fig. VII.6

a) Signs of deterioration on anode wire surface due to extensive sparking caused by contaminated drift gas.

b) Magnified section of wire from a). On the right a new wire for comparison

CHAPTER VIII. - DISCUSSION AND FUTURE CONSIDERATIONS

The tested multi-wire drift chambers (MMDC), due to the modular design, have proven to be a capable and flexible system. "In beam" tests, performed under conditions of a "real" experiment, showed the MMDC's to have high rate capability and very good spatial resolution for the coordinate perpendicular to the sense wires. Even though the charge-division read out techniques were not pursued very far, mainly because of field deficiencies in the respective drift cells and the lack of suitable amplifiers, the achieved resolution along the sense wires is comparable to the second-coordinate resolution of the presently used MWPC's.

Experiments using the QQD spectrometer, which require little or no vertical resolution at the target spot, can be run with the existing MMDC8 chamber exactly as it was set up and mounted for the testing in this thesis. There are big advantages over the 2 front MWPC set-up: much higher rate capability, reduced multiple scattering as two window foils are eliminated and the spectrometer itself can run in vacuum.

With the existing modules, one can also build a detector for experiments which do need vertical resolution by installing two 6-wire MMDC's, one of which is rotated by 90 degrees, at the front end of the spectromenter. This will provide a system which, in addition to the advantages outlined above, offers significantly improved resolution at

the target spot both in the horizontal and vertical direction. Considerations would have to be given to the space available between the spectrometer and the target chamber as well as to the decoupling of the electric fields from the two MMDC's inside the gas container.

A logical extension of the present MMDC system kit would be the construction of larger sized module frames. Multiple anode wire planes make it possible to build drift chambers of any size. A suggestion with regard to QQD spectrometer is to build modules of a size suitable to be placed into the WC3 position. As long as the maximum drift space is kept at 25 mm and the depth of each drift cell remains at 4 mm, MMDC's built with these units will have a similar performance to the ones which have now been tested. The QQD spectrometer could then be run with e.g. a four-wire MMDC at the front end (WC1) and another four-wire MMDC at the WC3 position. Extremely high horizontal and vertical resolutions could be obtained, since horizontally a trajectory can be fitted through eight data points. Vertically, four data points would be available over a large baseline if again only the first and last wire of each chamber is read out via charge division.

The electric drift field in the new modules can be considerably improved by first changing the wire spacings on the type "A" boards from 10 mm to 2 mm, and secondly, by placing two closely spaced wires in front of each anode plane. These wires have to be at the same potential as the anodes (see Fig. VIII.1).

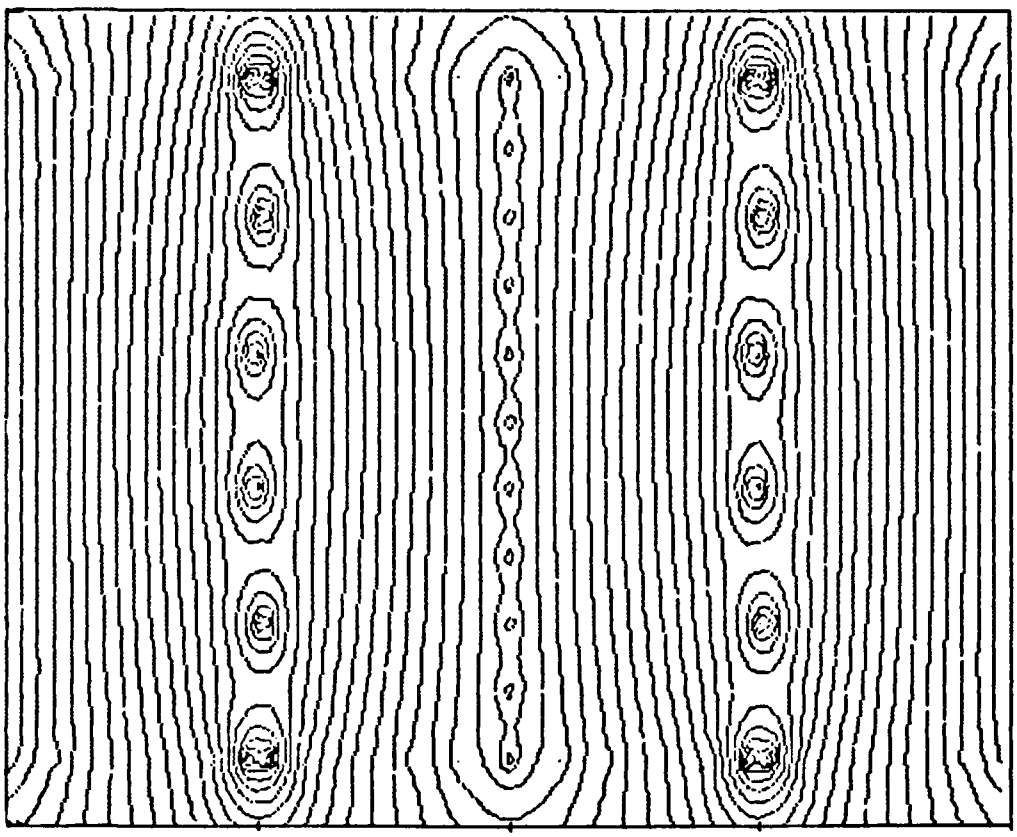

Fig. VIII.1 Calculated field map for the improved proposed modular system

The big improvement in the resolution due to the addition of Helium to the Argon-Ethane gas mixture should be further investigated. Helium is normally not used as a component in drift gas mixtures. Therefore, systematic measurements of chamber resolution as a function of Helium contents of three component gas mixtures are necessary to establish and optimize the findings of this work.

Finally, the most significant improvement for any of those drift chambers would be the implementation of Charge Coupled Devices (CCD's) for all wire read outs, since this would render the preamplification of the anode signals obsolete.

APPENDIX - MAXIMUM LIKELIHOOD METHOD

Call $\xi_i = \xi_i(a_1, a_2, \ldots, a_n)$ the "theoretical" expression for x_i, where the a_m are a set of parameters. In this case ξ_i are linear functions of the parameters a_m:

$$\xi_i = \sum_{m=1}^{2} c_{im} a_m \qquad i = 1,..,6$$

Then build a "data vector" X

$$X_m = \sum_{i=1}^{N} \frac{c_{im}}{\sigma_i^2}$$

and a "measurement Matrix" M

$$M_{ml} = \sum_{i=1}^{N} \frac{c_{im} c_{il}}{\sigma_i^2} = M_{lm}$$

Then solve for $a = M^{-1}X$ (M is now a 2x2 matrix)

REFERENCES

[1] F. Sauli, Principles of Operation of Multi Wire Proportional and Drift Chambers, CERN Report 77-09 (1979)

[2] G. Charpak, F. Sauli, High Resolution Electronic Particle Detecors CRN-EP (1984)

[3] F. Sauli, Limiting Accuracies in Multiwire Proportional and Drift Chambers, Wire Chamber Conference, Vienna (1978)

[4] E.W. McDaniel, E.A. Mason, The Mobility and Diffusion of Ions in Gases, Wiley & Sons, New York (1973)

[5] E. Townsend, Electrons in Gases, Hutchinson, London (1947)

[6] V. Palladino, B. Sadoulet, Nucl.Inst.Meth. 128, 323 (1979)

[7] L.G. Christophorou, D.L. McCorkle, D.V. Maxey, J.G. Carter, Nucl.Inst.Meth. 163, 141 (1979)

[8] A. Breskin, G. Charpak, B. Gabioud, F. Sauli, N. Trautner, W. Duniker, W. Schultz, Nucl.Inst.Meth. 119, 23 (1974)

[9] A. Peisert, F. Sauli, Drift and Diffusion of Electrons in Gases: A Compilation, CERN Report 84-08 (1984)

[10] F. Villa, Nucl.Inst.Meth. 217, 273 (1983)

[11] A.H. Walenta, Nucl.Inst.Meth. 217, 65 (1983)

[12] C.W. Fabjan, J. Lindsay, F. Piuz, F. Ranjard, E. Rosso, A. Rudge, S. Serednyakov, W.J. Willis, H.B. Jensen, F.O. Petersen, Nucl.Inst.Meth. 156, 267 (1978)

[13] S. Bartalucci, R.Bertani, S. Berolucci, M. Cordelli, R. Dini, P. Giromini, H. Pallotta, A. Rutili, A. Sermoneta, M. Spadoni Nucl.Inst.Meth. 192, 223 (1982)

[14] D.M. Binnie, Nucl.Inst.Meth. 192, 231 (1982)

[15] J.L. Alberi, V. Rakeka, IEEE Trans.Nucl.Sci., NS-23, No1, 251 (1976)

[16] F. Schneider, CERN Report 82-06 (1982)

[17] K.W.D. Ledingham, C. Raine, K.M. Smith, A.M. Campbell, M. Towrie, C. Trager, C.M. Houston, Nucl.Inst.Meth. 225, 319 (1984)